Lab on a Chip

CRITICAL REVIEW

View Article Online
View Journal | View Issue

Cite this: *Lab Chip*, 2023, **23**, 982

Recent microfluidic advances in submicron to nanoparticle manipulation and separation

Samith Hettiarachchi, [a] Haotian Cha,[a] Lingxi Ouyang,[a] Amith Mudugamuwa, [b] Hongjie An, [a] Gregor Kijanka,[a] Navid Kashaninejad, [a] Nam-Trung Nguyen *[a] and Jun Zhang *[a]

Received 27th August 2022,
Accepted 31st October 2022

DOI: 10.1039/d2lc00793b

rsc.li/loc

Manipulation and separation of submicron and nanoparticles are indispensable in many chemical, biological, medical, and environmental applications. Conventional technologies such as ultracentrifugation, ultrafiltration, size exclusion chromatography, precipitation and immunoaffinity capture are limited by high cost, low resolution, low purity or the risk of damage to biological particles. Microfluidics can accurately control fluid flow in channels with dimensions of tens of micrometres. Rapid microfluidics advancement has enabled precise sorting and isolating of nanoparticles with better resolution and efficiency than conventional technologies. This paper comprehensively studies the latest progress in microfluidic technology for submicron and nanoparticle manipulation. We first summarise the principles of the traditional techniques for manipulating nanoparticles. Following the classification of microfluidic techniques as active, passive, and hybrid approaches, we elaborate on the physics, device design, working mechanism and applications of each technique. We also compare the merits and demerits of different microfluidic techniques and benchmark them with conventional technologies. Concurrently, we summarise seven standard post-separation detection techniques for nanoparticles. Finally, we discuss current challenges and future perspectives on microfluidic technology for nanoparticle manipulation and separation.

1 Introduction

Submicron (0.10–1.0 μm) and nanoparticles (1.0–100 nm) such as extracellular vesicles (EVs),[1] bacteria,[2] viruses,[3] metal,[4] carbon,[5] and polymer nanoparticles,[6] *etc.* have broad

[a] *Queensland Micro- and Nanotechnology Centre, Griffith University, Nathan, Queensland 4111, Australia. E-mail: nam-trung.nguyen@griffith.edu.au, jun.zhang@griffith.edu.au*
[b] *University of Moratuwa, Katubedda 10400, Sri Lanka*

Samith Hettiarachchi

Samith Hettiarachchi received his honours degree in engineering (mechanical engineering) from the University of Moratuwa, Sri Lanka. He is currently a Ph.D candidate at Queensland Micro- and Nanotechnology Centre (QMNC), Griffith University, Australia. His research focuses on developing mechanisms for submicron to nanoparticle manipulation, focusing, and separation using microfluidics. His research interests are microfluidics, lab-on-a-chip, inertial microfluidics, viscoelastic microfluidics and computational fluid dynamics.

Haotian Cha

Haotian Cha received his bachelor's degree in engineering from Nanjing University of Science and Technology (NUST) and master's degree in engineering from the University of New South Wales (UNSW). He currently holds a position as a Ph.D. candidate in Queensland Micro and Nanotechnology Centre (QMNC) at Griffith University, Australia. His leading research focuses on developing innovative Multiphysics Microfluidics technology, especially inertial microfluidic technology for flexible cell focusing and separation. His research interests include dielectrophoresis (DEP), hydrophoresis, inertial microfluidic technology, and the development of lab-on-a-chip biomedical applications.

applications in disease diagnostics, drug delivery and material synthesis. The capability to manipulate and separate these tiny particles for isolating and enriching a specific population with uniform properties (*e.g.*, size, shape, and charge) is critical for these applications. For example, exosomes, a subset of EVs released from cells, have been recognised as an essential biomarker for diagnosing various diseases and monitoring therapy efficiency.[7] Exosome-containing biological fluids carry other EVs, such as microvesicles (MVs), apoptotic bodies and macromolecules (*e.g.*, proteins, proteases and nuclease), which may interfere with the analysis of exosomes. Therefore, efficient isolation and purification of exosomes from biological liquids have become increasingly important.[8] Moreover, the size fractionation of nanoparticles from the synthesised nanoparticles of broad size distribution is essential for practical applications because the functions and toxicities of nanoparticles are size-dependent.[9–11]

Many technologies have been developed for separating and concentrating nanoparticles, including ultracentrifugation,[12,13] ultrafiltration,[14] size exclusion chromatography,[15] precipitation,[16] and immunoaffinity capture.[17] Ultracentrifugation is the most common method for separating and purifying nanoparticles. The particles deposit on the bottom of the tube by centrifugal force induced by an ultra-high rotational speed. Furthermore, ultrafiltration and size exclusion chromatography use nanostructures on the membranes or columns to separate particles based on their size. In addition, the precipitation technique allows particles to aggregate by modifying the surface chemistry of nanoparticles with a solvent. Immunoaffinity capture utilises immobilised antibodies to selectively bind target particles through specific antigen interactions. These conventional techniques have high separation efficiency, ease of use, high yield and good reproducibility.[7] However, they suffer from several notable limitations, such as longer processing time, membrane clogging, high cost, low purity, or risk of damaging biological particles.[18] Therefore, extensive research efforts have been carried out to overcome these bottlenecks.

Microfluidics, the science of manipulating fluids in channels with dimensions of tens of micrometres, has emerged as a promising technology platform with many applications in chemistry, biology, medicine and physical science.[19] Benefiting from the precise control of fluid flow in microchannels, microfluidic technology offers an unprecedented resolution for manipulating and separating micro and nanoparticles.[20] Microfluidic techniques are broadly categorised as active and passive methods based on the origin of manipulating forces.[21] Active techniques use an external force field such as acoustic,[22] electric,[23] magnetic,[24] or optical[25] to precisely control particles. In contrast, the passive methods do not use any physical fields other than the intrinsic hydrodynamics and channel geometry. Examples of passive methods are inertial microfluidics,[26] deterministic lateral displacement,[27] microfluidic filtration,[28] pinched flow fractionation,[29] and viscoelastic microfluidics.[30]

Both active and passive methods have merits and demerits in particle manipulation. Active methods precisely control the particles with varying external forces in real time.[31] However, since they require a longer time to be exposed to the force field, the flow rate is generally slow, resulting in a relatively low throughput. In contrast, passive microfluidic devices for particle manipulation are simple, easy to operate and provide a relatively high throughput. Nevertheless, the controllability and accuracy are generally lower than active microfluidic techniques.[32] A recent trend is integrating multiple active and passive methods to overcome the

Nam-Trung Nguyen

Nam-Trung Nguyen received his Dipl-Ing, Dr Ing, and Dr Ing Habil degrees from Chemnitz University of Technology, Germany, in 1993, 1997, and 2004, respectively. From 1999 to 2013, he was an Associate Professor at Nanyang Technological University in Singapore. Since 2013, he has served as a Professor and the Director of Queensland Micro- and Nanotechnology Centre of Griffith University, Australia. He is a Fellow of ASME and a Senior Member of IEEE. His research is focused on microfluidics, nanofluidics, micro/nanomachining technologies, micro/nanoscale science, and instrumentation for biomedical applications. One of his current research interests is developing flexible and stretchable systems with bio interface.

Jun Zhang

Jun Zhang is currently an ARC DECRA fellow at Queensland Micro- and Nanotechnology Centre, Griffith University, Australia. He received his bachelor degree in engineering with an Outstanding Graduate Award from the Nanjing University of Science and Technology (NUST), China, in 2009, and received a PhD degree in Mechanical Engineering from the University of Wollongong, Australia, in 2015. His research exploits passive fluid inertia, fluid rheology and channel geometry, active force fields (electrical, acoustic and magnetic), and combinations for accurate manipulation and separation of micro/nanoparticles in microfluidics and explores their applications.

limitations of each technique.[33] To date, microfluidic techniques have been employed for manipulating, focusing and isolating various biological, metal and polymer nanoparticles for disease diagnostics, drug delivery, therapeutics, material synthesis, *etc.*[34–36]

Although a few recent literature review articles summarised the development of microfluidic technology for isolating specific bio nanoparticles such as EVs and exosomes,[7,20,37–39] this review paper aims to study the topic more comprehensively from a fundamental technological aspect to cover broad particle types and to provide an update on the latest technology developments. This paper first summarises the conventional techniques for the manipulation and separation of nanoparticles. Then, we elaborate on the current development of microfluidic technology based on the classification of active, passive, and hybrid microfluidics. We explain the physics of each manipulating force, the device design, working mechanism and applications. We also compare and discuss the advantages and limitations of the reported microfluidic technologies and compare them with conventional technologies. Concurrently, we summarise the seven most typical detection techniques for nanoparticles. Fig. 1 shows an overview of this paper, covering the scope of nanoparticle manipulation, separation, and detection. Lastly, we discuss the current challenges in the field and perspectives on future developments of microfluidic technology on nanoparticle separation.

2 Conventional techniques

Many technologies have been developed to manipulate and separate nanoparticles. Instead of exhaustively listing all

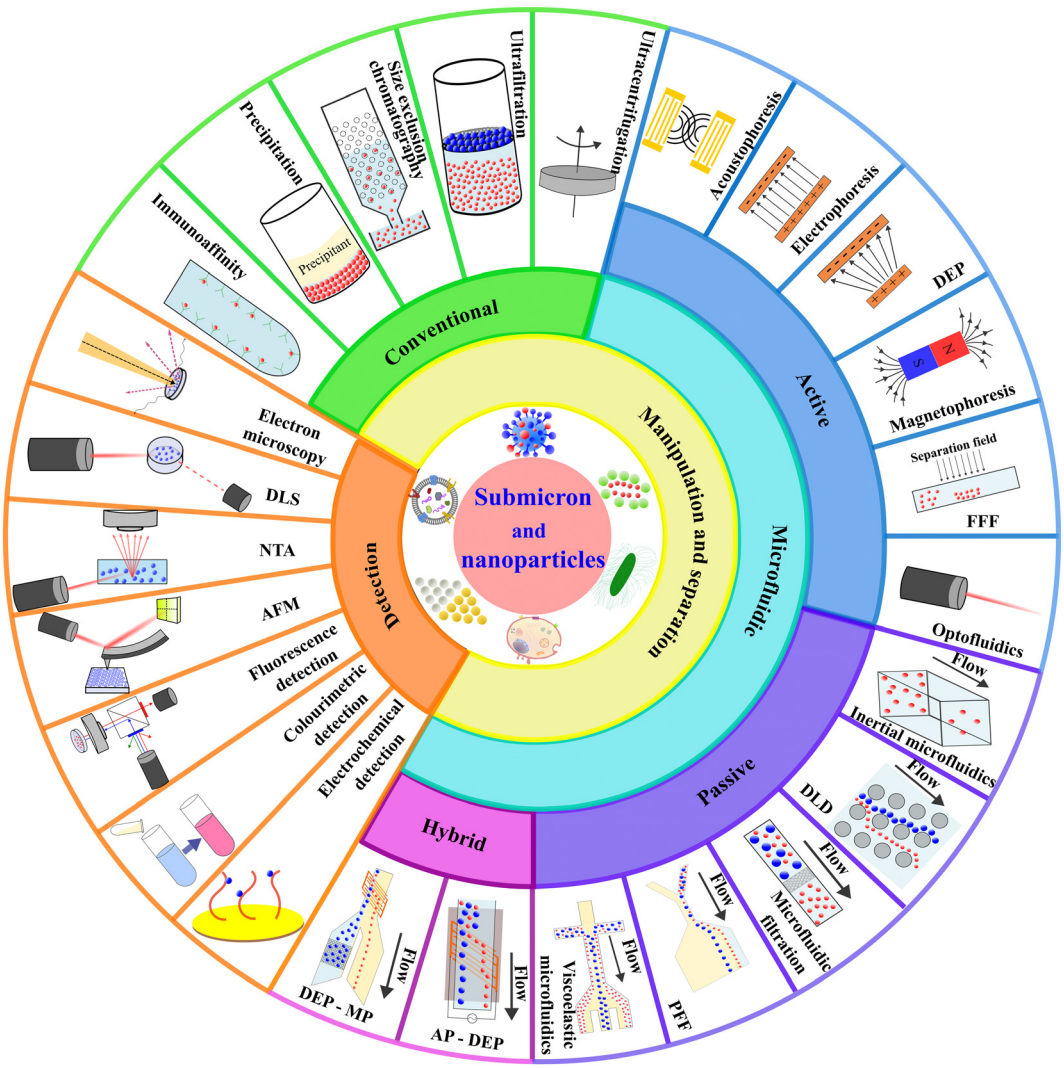

Fig. 1 An overview of submicron and nanoparticle manipulation, separation and detection techniques. Manipulation and separation can be mainly categorised as conventional and microfluidic technologies. Microfluidic technologies can be further subdivided into active, passive and hybrid techniques according to the manipulating forces. Abbreviations are DEP (dielectrophoresis), FFF (field flow fractionation), DLD (deterministic lateral displacement), PFF (pinched flow fractionation), AP–DEP (acoustic–dielectrophoresis), DEP–MP (dielectrophoresis–magnetophoresis), AFM (atomic force microscopy), NTA (nanoparticle tracking analysis), and DLS (dynamic light scattering).

Table 1 Summary of submicron and nanoparticle manipulation and separation techniques

	Technique	Principle	Particle size	Particle types	Separation efficiency	Throughput	Merits	Demerits	Ref.
Conventional techniques	UC	Centrifugal force by rotation	50–200 nm	Exosomes, polymersomes, gold nanoparticles	23–70%	10^6–6×10^8 cells per h	High throughput	Low yield, time-consuming, need for specialised equipment	12, 44, 48, 74
	UF	Membrane pore size	50–250 nm	Exosomes, natural organic matters	70–82%	0.5–1.6 ml min^{-1}	High separation efficiency, simple operation	Membrane clogging, possibility of damage due to shear stress	14, 54, 55
	SEC	Different elution speeds in a porous medium	50–200 nm	Exosomes, vesicles, gold nanoparticles, quantum dots	80–90%	25–250 μl min^{-1}	Shorter processing time, small sample volume, good reproducibility	Need for specialised equipment, possible adsorption to the stationary phase	53, 56, 58–60
	Precipitation	Converting a solution into a solid	50–150 nm	EVs, viruses	28–85%	0.35–8 μl min^{-1}	Less expensive, can process large sample volume, high throughput, easy integration with others	Time-consuming, co-precipitation of non-target particles, potential interference with the biological functions	16, 55, 66
	Immunoaffinity capture	Capturing by tagging antibodies	30–200 nm	Exosomes, EVs	—	4–160 μl min^{-1}	High specificity and purity	Low yield, time-consuming, high cost	17, 58
Active microfluidic techniques	AP	Acoustic radiation force	100–900 nm	MVs, bacteria	>90%	4–80 μl min^{-1}	High separation efficiency, contactless, highly controllable, biocompatible, wide versatility	Complex fabrication, low throughput, induced thermal energy	78, 92, 103
	Electrophoresis	Electrostatic force	3.5–150 nm	Exosomes, gold nanoparticles	65–98%	2–40 μl min^{-1}	High separation efficiency, highly controllable	Induce thermal energy, electrochemical reaction	4, 115, 120, 123
	DEP	Interaction of electrical polarisation and a non-uniform electrical field	50–490 nm	Exosomes, viruses, bacteria, polystyrene particles	77–83%	3–16 μl min^{-1}	High separation efficiency, controllable, minimum particle damage, high throughput	Require a strong electric field, joule heating, electrochemical reaction	79, 80, 83, 138
	MP	Magnetic force	5–200 nm	EVs, bacteria	80–90%	0.3–1000 μl min^{-1}	High throughput, contactless, low cost, non-contact, no heat generation	Time-consuming and labour-intensive sample preparation, exposure to the paramagnetic medium may affect the integrity of biomolecules	2, 147, 151
	FFF	Perpendicular force field to the flow	5–250 nm	Exosomes, gold nanoparticles, nanocolloids	90%	45–400 μl min^{-1}	High separation efficiency, high throughput, versatility by using various force fields	Longer setting up time, the limitation of the external force fields	162, 166, 170
	Optofluidics	Optical radiation scattering and gradient force	50–200 nm	Gold nanoparticles, silver nanoparticles, yeast cells	—	100–300 particles per min	High separation efficiency, precise controllability	Low throughput, induce thermal energy affects biocompatibility	172, 176, 177
Passive microfluidic techniques	Inertial microfluidics	Inertial lift and Dean drag forces	0.2–2 μm	EVs, polystyrene particles	15–97%	80–100 μl min^{-1}	High throughput, simple, good biocompatible	Inertial forces are weak, low separation resolution	180, 202

Table 1 *(continued)*

Technique	Principle	Particle size	Particle types	Separation efficiency	Throughput	Merits	Demerits	Ref.
DLD	Particles displace differentially in tilted pillar array	51 nm–1.5 μm	EVs, polystyrene particles	50–98.5%	0.1–0.2 nl min^{-1}	Simple, easy to operate, high separation resolution	Low throughput, channel clogging, high fabrication cost	185, 217, 254
Microfluidic filtration	Nano membrane in microfluidics	30–200 nm	Exosomes, viruses	73–89%	40–500 μl min^{-1}	High separation efficiency, simple, easy to operate	Membrane clogging, possible damage due to shear stress	188, 220, 222, 224
PFF	Pinching particles with hydrodynamic flows	30 nm–2 μm	EVs, viruses, polystyrene particles	82–90%	0.1–2.8 μl min^{-1}	Simple design, easy fabrication	Low throughput and efficiency, significant sample dilution by secondary flow	189, 190, 233
Viscoelastic microfluidics	Elastic force due to imbalance of normal stresses in a viscoelastic fluid	49 nm–2 μm	EVs, polystyrene particles	55–95%	90–1300 μl min^{-1}	Simple, higher separation resolution, low-cost biocompatible	Low throughput, potential contamination	191, 249, 250
Hybrid microfluidic techniques	DEP–MP	Connection of DEP and MP in a serial manner	500 nm	Bacteria	95.6–99.74%	2.5×10^7 cells per h	High separation efficiency, high throughput, sort multiple particles	Complex fabrication, time consumption	251
	AP–DEP	Force coupling of AP and DEP	300–500 nm	Exosomes, polystyrene particles	81–95%	0.75–3 μl min^{-1}	High separation efficiency, high precision	Induce thermal energy	252, 253

these technologies, we focus on the five most common technologies for nanoparticle separation: ultracentrifugation, ultrafiltration, size exclusion chromatography, precipitation, and immunoaffinity capture. Following this, we discuss their primary working principle and compare the technological features such as manipulating particle size and type, separation performance, throughput, *etc.*, Table 1.

2.1 Ultracentrifugation

Ultracentrifugation (UC) is predominantly used to separate particles based on particle size, shape, and density.[40] Particles deposit due to the centrifugal force induced by ultra-high rotational speed. UC generally uses a rotational speed of as high as 100 000–200 000*g* to separate nanoparticles such as exosomes.[41] Differential centrifugation and density gradient ultracentrifugation (DGUC) are two main modes of UC.[42] In differential centrifugation, multiple fractions within a mixture can be separated using differential centrifugation speeds.[13] The larger and denser particles form a sediment at a relatively lower rotational speed and are isolated from the mixture. A higher centrifugation speed is subsequently applied and isolates smaller and lighter particles from the supernatant, Fig. 2(A).[43] In DGUC, solutions with different densities are loaded into the centrifugal tube to create a density gradient medium.[44] During the ultracentrifugation, particles move through the medium and are retained where their densities match the surrounding medium due to the balance between centrifugal and buoyancy forces. Particles with various densities can be separated by differential fraction collection.[45] UC has been widely employed and is considered the gold standard for particle separation.[46,47] However, UC suffers from low yield, long processing time, inconsistent outcomes, the necessity for a large sample volume, high-cost equipment, and skilled labour requirement.[48–50] Moreover, biological particles may be damaged by forces induced by high rotational speed, which diminishes downstream analysis.[51]

2.2 Ultrafiltration

Ultrafiltration (UF) utilises porous membranes to separate particles based on the membrane pore sizes.[52] The particles are infiltrated through the membrane by applying pressure or centrifugation.[53,54] Particles larger than the cut-off size are trapped on the membrane while smaller particles can pass through it, Fig. 2(B).[36] UF is a faster alternative to UC and provides a higher yield with increasing isolation efficiency.[55] However, particles experience a relatively high stress during the passage through the membrane pores, potentially damaging the morphology or functionality of particles. The large particles trapped in the membrane may cause clogging. Membrane clogging prevents the passage of desired particles from crossing the membrane and lowers the throughput and recovery rate.[14] Moreover, the co-existence of particles of similar size reduces the purity of target particles.[38]

2.3 Size exclusion chromatography

Size exclusion chromatography (SEC) is a size-based particle isolation technique that uses a stationary phase of porous beads with defined pore size. Particles smaller than the pores of porous beads can travel through them, whereas larger particles cannot penetrate through and can only move between the porous beads, Fig. 2(C). The travelling time for smaller particles is longer than the larger particles, resulting in a later elution.[56] This technique is easy to use and low cost and has shown a high reproducibility in isolating nanoparticles with low volume.[57,58] However, SEC needs specialised equipment, and purity may be compromised due to the coexistence of particles of similar sizes.[59] Irreversible adsorption of nanoparticles to the stationary phase is another drawback of this technique.[15] Recent approaches combining SEC and UF have significantly enhanced the purity of isolated exosomes.[60]

2.4 Precipitation

Precipitation converts particles in solution into a solid phase by transforming the substance into its insoluble form or oversaturating the solution.[61] Polymer-induced precipitation is employed to isolate biological particles such as exosomes and EVs. The water-soluble polymer such as polyethylene glycol is added to the sample and incubated for a period of time, Fig. 2(D). The precipitated EVs or exosomes form sediment in the form of a pellet after low-speed centrifugation or filtration.[53] Precipitation is also used to synthesise non-biological nanoparticles.[62,63] For example, ionic metals are converted to an insoluble form by a chemical reaction of a soluble metal and a reagent. Subsequently, the formed metal particles can be removed by filtration.[64] Precipitation-based isolation is low-cost as it does not need special equipment requirements.[16,53,65] This technique can process large sample volumes and be easily integrated with other separation methods.[39] However, the precipitation reagents may interfere with the biological characteristics of particles.[66,67] Co-precipitation of non-target particles can cause the contamination of target particles, such as co-precipitation of protein and polymeric substances during exosome precipitation using polymer solutions.[7]

2.5 Immunoaffinity capture

Immunoaffinity capture is widely employed to isolate biological particles from a mixture based on the specific interaction of an antibody and an antigen.[17] The surfaces of many bioparticles comprise antigens that can be bound exclusively by particular antibodies.[68] The antibodies can be immobilised on the surface of a solid phase, such as magnetic beads, plates, and chromatography matrices. Due to the specific binding between the antibody and antigen, the target bioparticles are immobilised on the solid phase. In contrast, unbound, non-specific particles are freely dispersed in the medium and can be eluted, Fig. 2(E).[69] Therefore, target bioparticles can be selectively isolated and concentrated.[70] For the isolation of exosomes, the most commonly utilised biomarkers are tetraspanins such as CD9, CD63, CD81, CD82, and CD151.[71–73] Immunoaffinity-based capturing methods provide a high separation specificity. Still, this method is challenged by relatively low yields, limited accessibility of particular antibodies, and potential damage to the biological particles.[38,74]

3 Active microfluidic techniques

Active microfluidic technologies utilise external force fields to manipulate and separate particles on top of the intrinsic hydrodynamic forces.[21] Acoustic, electric, magnetic, and optical force fields are the most commonly used in active microfluidics.[75] Due to their versatility and high controllability, active microfluidic technologies have been tailored to process many submicron and nanoparticles, including exosomes,[76,77] bacteria,[2,78,79] viruses,[80] platelets,[81] polystyrene and gold nanoparticles,[4,82,83] *etc.* In the following, we will explain the physics of each manipulation force, the current status of the research, the working mechanism of the reported devices, and their application to the manipulation of submicron and nanoparticles.

3.1 Acoustophoresis

Acoustophoresis (AP) is defined as the movement of particles by sound waves.[84] In this technique, ultrasound waves exert acoustic radiation forces on particles, and particles migrate toward the acoustic pressure nodes or antinodes based on the relative compressibility of particles and fluids. The strength of the acoustic radiation force on a particle depends on the particle size, density, and compressibility.[85] The magnitude of the acoustic radiation force (F_R) acting on a spherical particle with a diameter of d can be expressed as:[86]

$$F_R = -\left(\frac{\pi^2 {P_0}^2 d^3 \beta_f}{12\lambda}\right) \varnothing(\beta,\rho) \sin(2kx) \quad (1)$$

$$\varnothing(\beta,\rho) = \frac{5\rho_P - 2\rho_f}{2\rho_P + \rho_f} - \frac{\beta_P}{\beta_f} \quad (2)$$

where P_0 is the acoustic pressure, β is the compressibility, ρ is the density, and subscripts f and p represent the fluid and the particle, respectively. λ is the wavelength, k is the wavenumber of the acoustic waves, and x is the distance from a pressure node. The acoustic contrast factor depends on the density and compressibility of the particle and fluid, which determines the direction of particle movement. If the contrast factor is positive ($\varnothing > 0$), particles move towards the pressure node. If the contrast factor is negative ($\varnothing < 0$), the particles migrate towards the antinode.[87]

Particle manipulation by an acoustic field has been widely known as acoustic tweezers.[88] Surface acoustic waves (SAWs)[89] and bulk acoustic waves (BAWs)[90] are the two main platforms for microparticle manipulation.[91–93] SAWs are mechanical waves travelling along a substrate surface, and they are generally induced by interdigitated transducers

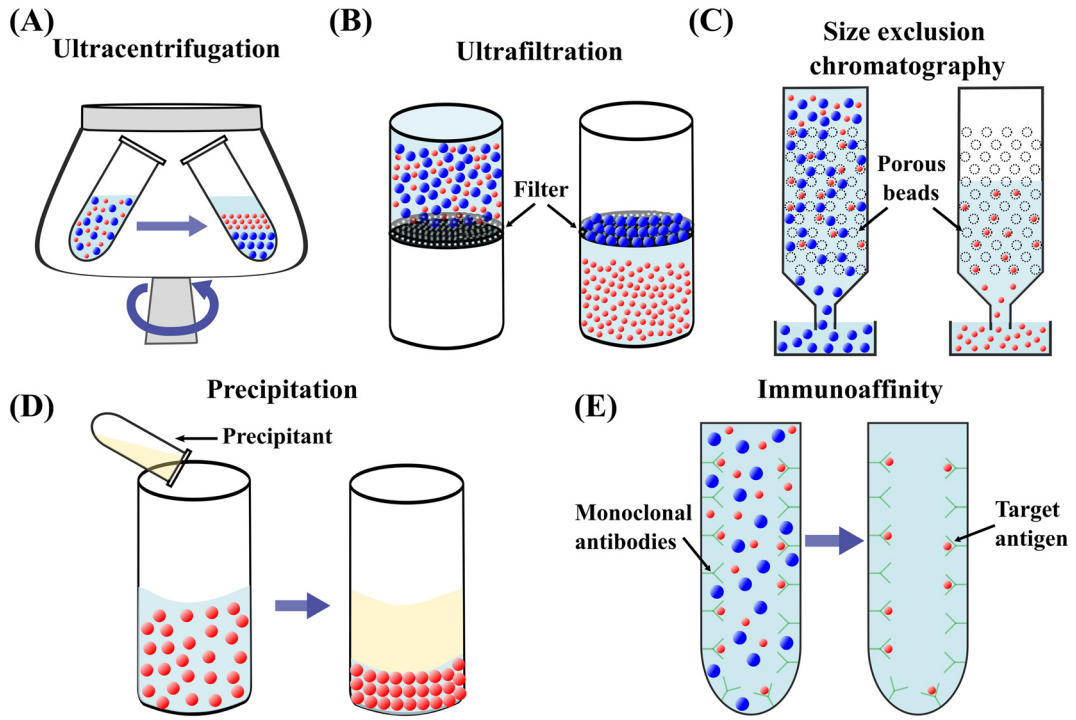

Fig. 2 Schematic diagrams of conventional techniques for submicron and nanoparticle separation. (A) Ultracentrifugation.[13] (B) Ultrafiltration.[53] (C) Size exclusion chromatography.[59] (D) Precipitation.[61] (E) Immunoaffinity capture.[17]

(IDTs) with different electrode shapes such as focused[94] and straight[95] on the surface of piezoelectrics.[96] SAWs can further be divided into standing surface acoustic waves (SSAWs) and travelling surface acoustic waves (TSAWs).[97,98] BAWs are the compressional waves propagating through a bulk material.[90] With an acoustic resonator, particles suspended in a medium can be effectively manipulated by BAW.[88,99] Acoustophoresis is simple, robust, contactless, and biocompatible for particle manipulation. This technique has been successfully applied for the separation and purification of submicron and nanoparticles such as platelets,[81] MVs,[100] lipid particles,[101] bacteria,[78,102] and polystyrene nanoparticles.[82]

Lee *et al.*[103] reported on an acoustic nanofilter system to separate MVs from biological samples using the SSAW principle. In their device, the two sheath flows pinched the sample to the middle of the microchannel at the inlet. Next, acoustic radiation force pulls larger MVs to the pressure nodes near two sidewalls, whereas the smaller MVs remained at the central flow due to the weak acoustic force, Fig. 3(A). The device isolated exosomes with diameters less than 200 nm from cell culture media and erythrocyte-derived vesicles from blood samples with a recovery rate of more than 80%. Meanwhile, using the same principle with tilted IDTs, a fractionation of nanoparticles of varying sizes could also be achieved.[11] 110 nm and 220 nm polystyrene particles were separated from 900 nm and 600 nm ones. The recovery rates of 110 nm and 220 nm particles were 90.6% and 85.6%, and the depletion ratios of 900 nm and 600 nm particles were 96.6% and 80.4%, respectively. Furthermore, the same group successfully isolated exosomes from undiluted blood with a purity of 98% by integrating two sequential tilted angle SSAW modules.[100] In this platform, the first module removed the larger blood components, such as red blood cells (RBCs), white blood cells (WBCs), and platelets. The second module in the downstream isolated exosomes from the remaining EVs. In addition to symmetric acoustic transducers where interdigitated electrodes are patterned symmetrically on the two sides of microchannels, asymmetric acoustic waves have also been reported. Collins *et al.*[82] developed a focused TSAW device that manipulates micro and nanoparticles using an asymmetric focused acoustic wave, Fig. 3(B). Different focus points for separating nanoparticles of 100 nm, 300 nm, and 500 nm diameters were observed regardless of their initial starting position.

In contrast to SAW, the BAW technique has rarely been studied for manipulating submicron and nanoparticles.[104,105] Ohlsson *et al.*[78,106] successfully utilised the BAW technique to separate and enrich bacteria from the blood. In their device, bacteria were first isolated from RBCs by acoustic force and then enriched using acoustic trapping. Due to the operational frequency range of BAW, separating nanoparticles is challenging for this technique.

In summary, acoustophoresis has been used in a wide range of applications in biomedical research, such as diagnostics and therapeutics.[104,107] In general, it possesses the advantages of being contactless, biocompatible, highly controllable, and versatile in submicron and nanoparticle manipulation. However, the processing throughput is relatively low, the fabrication process for these devices is complex, and the induced thermal energy may deteriorate

the performance of the devices. Moreover, since biological fluids contain components of similar size and acoustic characteristics, acoustic separation of these components may be challenging.[108]

3.2 Electrophoresis

Electrophoresis is the relative motion of charged particles over fluid in an electric field.[109] Due to the electrostatic force, charged particles are drawn towards the oppositely charged electrode, whereas the field does not affect uncharged particles. The electrophoretic force (F_{EP}) acting on a spherical particle with a radius a can be expressed as:[110]

$$F_{EP} = 6\pi\zeta_p\varepsilon_m aE \quad (3)$$

where ζ_p is the zeta potential of the particle, ε_m is the permittivity of the medium, and E is the electric field. Electrophoresis can be classified into capillary electrophoresis (CE), gel electrophoresis (GE), dielectrophoresis (DEP), and field-flow fractionation.[111] Due to the versatility of separation modes, electrophoresis has been widely employed for the separation of various biochemical species,[112–114] exosomes,[77,115,116] and nanoparticles.[4,117–119]

Mogi *et al.*[77] developed a microfluidic device capable of damage-less handling of exosomes using an ion-depletion zone. A direct current (DC) voltage of 100 V was applied between two microchannels to create an ion depletion region through a Nafion membrane. This region acts as a barrier against any charged particles. Since exosomes are negatively charged, they are pushed away by the ion depletion zone.

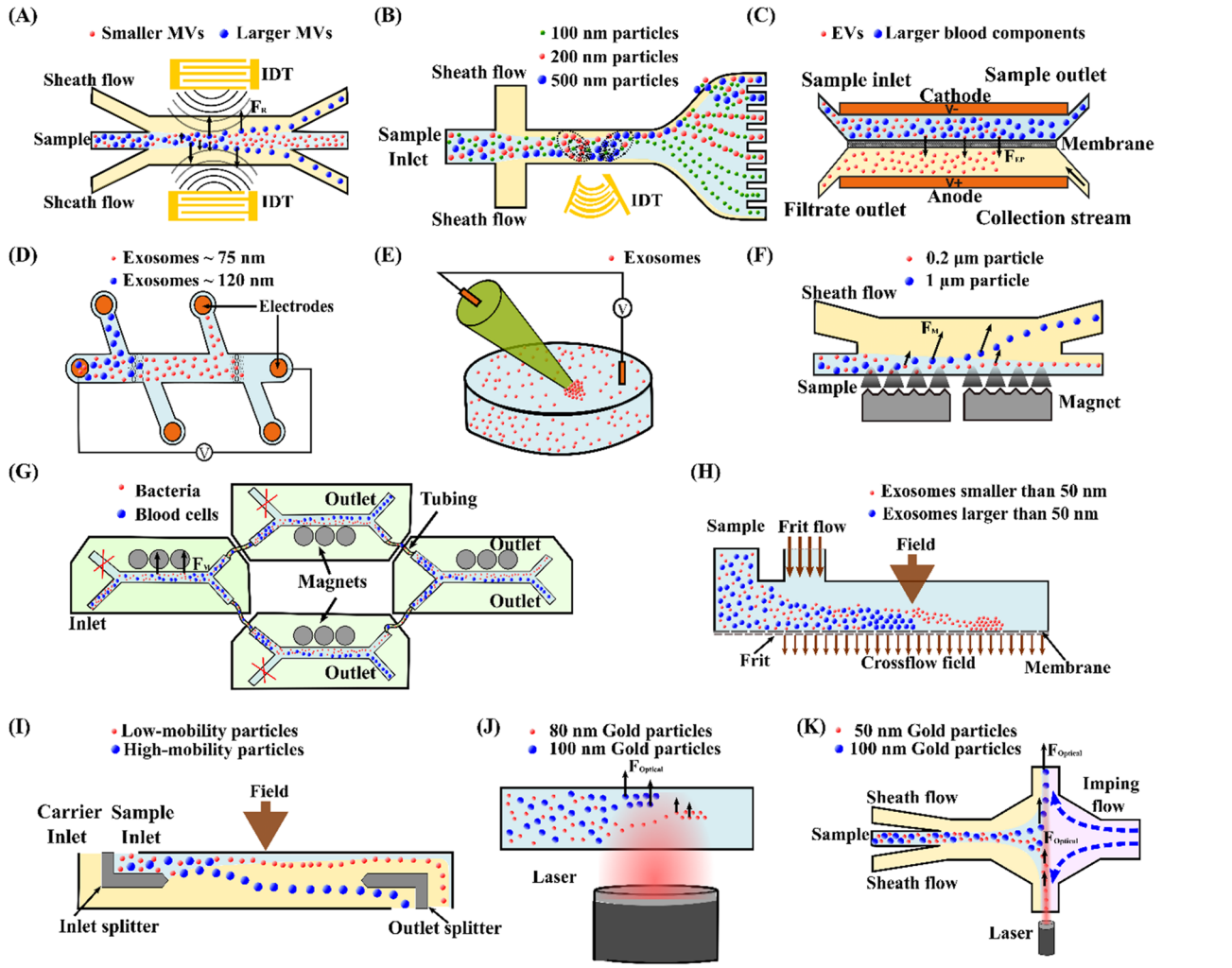

Fig. 3 Active microfluidic techniques for manipulation, focus, and separation of submicron and nanoparticles. (A) Separation of MVs by acoustophoresis.[103] (B) Focused TSAW device for separating 100 nm, 200 nm and 500 nm polystyrene particles.[82] (C) Isolation EVs from whole blood by DC electrophoresis.[115] (D) Simultaneous capture and separation of different subpopulations of exosomes by DC insulator-based dielectrophoresis.[137] (E) Entrapment of exosomes by a low voltage nanopipette DEP device.[76] (F) Separation of 0.2 μm and 1 μm fluorescence polystyrene particles by magnetophoresis.[146] (G) Separation of bacteria by integrating multiple magnetophoresis devices.[2] (H) Size fractionation of exosomes by field-flow fractionation.[166] (I) SPLITT device for improved fractionation of cells/particles.[168] (J) Trapping of 80 nm and 100 nm gold particles by optofluidics.[176] (K) Optofluidic sorting of gold nanoparticles of 50 nm and 100 nm diameters.[172]

Using this technique, the team achieved an exosome yield of 98% with less damage than the conventional techniques. In addition, a combination of DC electrophoresis and a membrane filter was proposed to isolate EVs from whole blood.[115] A DC voltage of 10 V was applied over two electrodes with a separation distance of 1.5 cm, Fig. 3(C). A porous monolithic membrane with pore sizes of less than 500 nm allows EVs to pass through the membrane between two electrodes. Furthermore, a similar technique has been used to separate EVs from proteins in the blood plasma.[120] The membrane pore size was 30 nm so that proteins could pass through the membrane, but the EVs were retained. This work recovered 65% of EVs, and 83.6% of the protein was removed within 30 minutes. Gold nanoparticles are used in biomedical imaging and diagnostics, but their cytotoxicity depends on particle size.[121] Thus, it is crucial to isolate monodisperse metallic nanoparticles.[122] Using commercially available CE equipment in an evaporative light scattering detector (ELSD), Bouri *et al.*[4,123] separated gold nanoparticles of 3.5 nm, 6.5 nm, and 10.5 nm.

In summary, electrophoresis is simple in design and controllable but requires trained users and tedious operation steps.[36] Moreover, direct contact between sample solution and electrodes and potentially excessive heat generation due to the high voltages may also affect biological components such as exosomes.[124]

3.3 Dielectrophoresis

Dielectrophoresis (DEP) is the movement of dielectric particles when subjected to a non-uniform electric field.[125] The force exerted on the particle depends on the dielectric properties of the particles and the suspending medium.[126,127] The actuating electric field can be alternating current (AC) or DC.[128] For a homogeneous spherical particle, the DEP force (F_{DEP}) is expressed as:[129]

$$F_{DEP} = 2\pi a^3 \varepsilon_m \, \mathrm{Re}[K(\omega)] \nabla |E_{rms}|^2 \quad (4)$$

where $\mathrm{Re}[K(\omega)]$ is the real part of the Clausius–Mossotti (CM) factor, ω is the electrical frequency, and E_{rms} is the root mean square of the electric field. The CM factor is defined as:[130]

$$K(\omega) = \frac{\varepsilon_p^* - \varepsilon_m^*}{\varepsilon_p^* + 2\varepsilon_m^*} \quad (5)$$

$$\varepsilon_p^* = \varepsilon_p - \frac{i\sigma_p}{\omega} \quad (6)$$

$$\varepsilon_m^* = \varepsilon_m - \frac{i\sigma_m}{\omega} \quad (7)$$

where ε^* is the complex permittivity, ε_p is the permittivity of the particle, and σ is the conductivity. In a DC electric field, since ω is zero, the CM factor is simplified as:[131]

$$K(0) = \frac{\sigma_p - \sigma_m}{\sigma_p + 2\sigma_m} \quad (8)$$

Depending on the CM factor, DEP is categorised as positive or negative DEP. If the permittivity or the conductivity of the particle is greater than that of the medium ($K(\omega) > 0$), it is called positive DEP, and particles move towards the maximum electric field. Conversely, if the polarisation of particles is lower than the medium ($K(\omega) < 0$), it is the negative DEP force that migrates particles towards the minima of the electric field.[125,132,133] Both the positive and negative DEP forces can be used to separate submicron and nanoparticles[83] and biomolecules, such as viruses,[80] bacteria,[79,134] and exosomes.[135,136]

Zhao *et al.*[83] developed a novel DC-DEP microfluidic device for continuous separation of nanoparticles with similar sizes but different electric properties (*i.e.* 140 nm polystyrene and 150 nm magnetic particles). The non-uniform electric field was generated using a pair of asymmetric orifices in their device. Particles experienced distinct positive and negative DEP forces due to different electrical conductivities and were separated into various outlets. Apart from the electrical properties, DC-DEP could also separate submicron particles by size. Ayala-Mar *et al.*[137] developed a DC insulator-based DEP (DC-iDEP) device to capture and separate two different subpopulations of exosomes by size, Fig. 3(D). The device has two different channel sections filled with oval-shaped insulating posts to trap the exosomes of diverse populations. The first post array has a gap space of 15 μm to trap exosomes with a mean diameter of 113.23 ± 10.34 nm, while the second array with 10 μm gap spaces was capable of trapping the exosomes with a mean diameter of 72.86 ± 8.71 nm. Successful trapping was achieved with an electric potential difference of 2000 V. After the trapping, electric stimulation was removed to release the exosomes, and a DC voltage of 200 V was applied to side channels to direct the released exosomes to the respective reservoirs by electroosmosis. In addition, an alternative approach was introduced by Shi *et al.*[76] by applying a significantly lower DC voltage (10 V cm^{-1}) across a glass nanopipette, Fig. 3(E). The device is capable of rapid entrapment of nanoparticles and exosomes. When a DC voltage was applied across the pipette, the particles suspended in the medium were attracted towards the pipette tip due to the balance between dielectrophoretic, electroosmotic, and electrophoretic forces. Exosomes from undiluted plasma, serum and saliva were isolated separately from four parallelly connected pipettes with a negative electrical polarity.[135]

Meanwhile, an AC electrokinetic (ACE) microarray device was developed to isolate various drug delivery nanoparticles with diameters between 100 nm and 200 nm from blood plasma.[35] A positive DEP force trapped particles at the electrode edges with a high electric field in the device. A washing buffer subsequently eluted the non-trapped

particles, and the particles held by DEP force could be released and collected by removing the AC electric field. Due to the distinct dielectric properties, the recovery of each type of drug delivery nanoparticle required a different AC electrical strength. Gel-filled nanoliposomes, hollow silica shells, empty nanoliposomes, and solid polymer nanoparticles were isolated at an electric voltage of 12 V_{pp}, 8 V_{pp}, 18 V_{pp}, and 15 V_{pp}, respectively. Later, the same group successfully applied the ACE microarray chip to isolate glioblastoma exosomes from 30–50 μl undiluted human plasma in less than 30 minutes.[138] Another study proposes utilising DEP to rapidly detect the dengue virus (DENV).[80] The microfluidic device consists of a guiding electrode and a capturing electrode. First, mouse anti-flavivirus monoclonal antibody (4G2) coated beads were infused into the device and captured on the electrode. Then the DENV-labelled fluorescent probe was injected to interact with 4G2-coated beads, so that the virus could be detected based on the fluorescence intensity. In addition, a periodically controlled positive DEP chip is developed to continuously isolate rare pathogenic bacteria from the blood.[79] The device is divided into three main sections: focusing, separation, and collection. The sample pinches towards the sidewall by a sheath flow in the focusing region. The bacteria experience a positive DEP force, but no net DEP force is exerted in WBCs in the separating region. The trajectory of bacteria is separated from that of WBCs. Finally, bacteria and WBCs are collected at distinct outlets in the collecting region. This device recovered 82.1% *E. coli*, 83.3% *S. aureus*, and 77.1% *P. aeruginosa* from WBCs.

The DEP technique is promising for manipulating biological particles with adequate controllability, easy operation, high efficiency, and minimum particle damage.[128,139] Furthermore, DEP is label-free and suitable for low-volume sample processing. However, DEP has challenges, such as creating non-uniform electric fields at the nanoscale to achieve precise, flexible, and large-scale manipulation of nanomaterials.[140] Moreover, microfluidic devices may suffer from the adhesion of particles and chemical reactions on the surfaces of electrodes, resulting in a reduction in the recovery yield. In addition, a strong electric field is needed to manipulate nanoparticles. However, an excessive electric field may affect the viability and functionality of bioparticles.[79]

3.4 Magnetophoresis

Magnetophoresis (MP) refers to the movement of particles relative to the fluid under an external magnetic field.[141] The magnetic field can either be generated by a permanent magnet or an electromagnet. The magnetic force (F_M) acting on a particle can be expressed as:[142]

$$F_M = \frac{V_p \times \left(\chi_p - \chi_f\right)}{\mu_0}(B\cdot\nabla)B \quad (9)$$

where V_p is the volume of the particle, χ_p is the magnetic susceptibility of the particle, χ_f is the magnetic susceptibility of the fluid, B is the magnetic flux density, ∇B is the magnetic flux gradient, and μ_0 is the permeability of the vacuum. The difference in magnetic susceptibilities of the particle and the fluid is critical for the induction of the magnetic force. When the χ_p is larger than χ_f, positive magnetophoresis occurs where the particle migrates towards the maximum magnetic field. In contrast, when χ_f is larger, the particle experiences negative magnetophoresis, where particles are attracted to the minimum magnetic field.[143] Positive magnetophoresis can directly manipulate particles with magnetic properties such as RBCs or cells labelled with magnetic beads. Negative magnetophoresis generally manipulates non-magnetic particles in a biocompatible magnetic medium.[144,145] Benefiting from the inherent properties of its simple, low cost, and non-contact nature, this technique has been used in a wide range of applications, including submicron and nanoparticle,[146] EV,[147] and bacteria detection.[2,148–150]

Zeng *et al.*[146] developed a magnetofluidic device to separate 0.2 μm-polystyrene particles from 1 μm particles using negative magnetophoresis. At the inlet region, sample flow is focused along the side of a magnetic pole array by a co-flowing sheath flow. Large (1 μm) particles experienced a more significant negative magnetophoretic force in the separation channel and were repelled further away than the small (0.2 μm) particles, Fig. 3(F). In order to generate an ultrahigh magnetic intensity and gradient for separating nanoscale particles, high-permeability alloys, on-chip integrated magnetic micro-pole arrays, and a strong external NdFeB permanent magnet were incorporated into the microfluidic device. Later, they modified the device to enhance the sample throughput by taking advantage of the separation space between both sidewalls.[147] In the modified device, the sheath flow symmetrically focused the sample flow along both sidewalls at the inlet. The high-permeability alloys, on-chip magnetic micro-pole arrays and permanent NdFeB magnets have been symmetrically patterned on both sides of the separation channel so that symmetric ultrahigh magnetic fields repelled nanoparticles toward the channel centre. They applied the device to separate small extracellular vesicles (sEVs) with dimensions 30–200 nm from the cell culture supernatant, and a recovery rate of 85.8% and purity of 80.45% were achieved. Using a similar ferrohydrodynamic technique, Liu *et al.*[151] successfully separated 30–150 nm exosome-like particles from a biological sample with a recovery rate of 94.3% and a purity of 87.9%. This work used a quadrupole configuration of four permanent magnets to provide both high magnetic flux density and gradient.

Furthermore, positive magnetophoresis has been used to isolate target bioparticles by magnetic labelling. Separating bacteria from blood cells is vital for rapidly diagnosing bloodstream-related infections.[152] Lee *et al.*[2] developed a microfluidic system to separate *E. coli* from blood using bis-Zn-DPA modified magnetic nanoparticles, which can bind to both Gram-positive and Gram-negative bacteria. 88% *E. coli* were removed in the first cycle, and complete removal was

achieved after the second cycle. Later the team enhanced the performance of the microfluidic platform by integrating multiple devices in series and parallel so that the separation could be completed in a single pass, Fig. 3(G). In addition, Oh *et al.*[150] proposed a novel magnetisable micropipette tip to separate *E. coli* by positive magnetophoresis. The microtip contains a nickel mesh with rectangular micropores, and a permanent magnet could instantaneously magnetise it. Bacteria labelled with magnetic nanoparticles were attracted and attached to the mesh. After washing off the non-targets and demagnetising the tip, the *E. coli* were recovered at a 90.5% recovery rate.

Magnetophoresis is advantageous in non-contact, high throughput isolation, low cost, has selective controllability, and minimal heat generation.[153–155] Despite the advantages, sample preparation for magnetophoresis is time-consuming and labour-intensive. The separation efficiency depends on the properties, such as the load capacity of the magnetic beads.[144] Furthermore, the accumulation of magnetic nanoparticles and prolonged exposure to the paramagnetic medium may also affect the integrity of biomolecules.[156]

3.5 Field-flow fractionation

Field-flow fractionation (FFF) is a chromatography-like technique that uses an external force field perpendicular to the main flow to fractionate particles, Fig. 3(H).[157] The external force can be hydraulic, thermal, electric, magnetic, or gravitational, and they can displace particles laterally to the side walls.[158] The migration speed of the particles is affected by the physical parameters of the particle, the applied force field and the parabolic flow profile.[159] Giddings first invented this technique in 1966.[160] FFF partially overlaps with the scope of other active or passive techniques. FFF has been successfully utilised to isolate and characterise biological and non-biological sub-micro and nanoparticles.[161–165]

The FFF technique has been used to separate EVs based on their hydrodynamic diameter. Kang *et al.*[166] developed a flow FFF to fractionate exosomes according to their hydrodynamic diameter, Fig. 3(H). The team created an asymmetrical fluid flow as the external field and accumulated particles at the bottom wall. When an external field was applied, the small particles were eluted earlier than the larger ones, resulting in the size-based separation of particles. Their device isolated exosomes larger than 50 nm and smaller than 50 nm, respectively. A similar study fractioned urine exosomes ranging from 28.2 ± 4.3 nm to 136.7 ± 27.9 nm in diameter. The results indicated that the exosome fractions obtained from urine samples of healthy donors differed from those of prostate cancer.[167]

In addition, the same principle was used to separate a gold nanoparticle mixture by Calzolai *et al.*[162] A cross-flow field separated 5 nm, 15 nm, and 45 nm gold nanoparticles from the nanoparticle mixture. Subsequently, a novel split-flow lateral-transport thin (SPLITT) technique was introduced by Giddings to improve cell/particle fractionation, Fig. 3(I).[168] In this approach, splitters were added to the inlet and outlet to direct the particles to different outlets while an external force field acted perpendicular to the flow direction. The inlet splitter prevents the carrier stream from being in contact with the sample until they are under the influence of the external force field. The acting force on the particles transferred them into the carrier medium. The outlet splitters divided the stream into two outlets, consequently enabling the collection of separate sample fractions. De Momi *et al.*[169,170] implemented this technique to fractionate colloids and particles in lake water, which facilitated the understanding of trace pollutant fate and behaviour in the environment. They were able to fractionate nanoparticles less than 10 nm to 250 nm.

Although FFF is advantageous in separating particles that differ in size, it can also sort particles differentiated by their mass, thermal, electrical, and magnetic characteristics since various physical forces can be employed. However, FFF has challenges such as a relatively long processing time for setting up and analysis, the inability to distinguish between differently shaped particles with the same mean hydrodynamic diameter or mass, and requiring optimisation at different external fields.[161]

3.6 Optofluidics

Holding and moving microscopic and sub-microscopic objects like atoms, nanoparticles and droplets using a focused laser beam is called optical tweezers, which Ashkin discovered in 1970.[171] The optical force that acts on a particle is the sum of the radiation scattering force and gradient force. The scattering force pushes the particle along the direction of the light, and the gradient force pulls the particles towards the highest intensity gradient. The induced optical force depends on the particle size, shape, and reflective index. Optical tweezers have been widely used in chemistry, physics, biology, and medicine.[172–175]

Nan *et al.*[176] trapped 150 nm silver nanoparticles and sorted 80 nm and 100 nm gold nanoparticles with the synchronisation of an optical phase gradient and fluid drag forces, Fig. 3(J). When the particle reaches the trapping plane, the optical line can tightly confine the nanoparticle in the perpendicular direction of the flow. Then a strong phase gradient creates a lateral force that balances the fluid drag force and traps the particle. Due to the size-dependent nature of optical and fluid drag forces, the 80 nm and 100 nm particles were trapped in an optical line with a distance of ~5 μm. Meanwhile, Wu. *et al.*[172] reported the separation of gold nanoparticles with different diameters (50 nm/100 nm and 100 nm/200 nm) in a continuous manner, Fig. 3(K). In this device, two sheath flows confined the sample to a narrow region, and a counter flow created a stagnation point from the opposite side. The larger particles were pushed to the buffer stream, whereas the smaller particles remained within the sample flow under a laser beam so that the particles

could be collected at two different outlets. Two-line 'Y'-shaped optical tweezers patterned in a microfluidic channel were developed to sort yeast cells of various sizes by tuning optical intensities and wavelengths.[177] The force acting on larger and smaller cells varies by the two-line tweezers in a way that the particles can be sorted into two different outlets. The optimal sorting was achieved when one line laser power was kept at 35 mW, while the second line laser power was altered from 100 to 190 mW.

Since light has better directionality and can be controlled precisely, it provides excellent efficiency in separating submicron and nanoparticles. Even though optofluidics can easily be integrated within a microfluidic device, heat generation during the operation limits applicability to biological particles due to biocompatibility concerns.[178] In addition, the throughput of optofluidics is relatively low since the optical force is generally weaker than other forces.

4 Passive microfluidic techniques

Passive microfluidic techniques utilise intrinsic hydrodynamic forces and channel geometry for particle manipulation. The reported passive microfluidic technologies for submicron and nanoparticle separation include inertial microfluidics,[179–182] deterministic lateral displacement,[183–185] microfluidic filtration,[186–188] pinched flow fractionation,[189,190] and viscoelastic microfluidics.[191–193]

4.1 Inertial microfluidics

Inertial microfluidics is a passive microfluidic technology that employs hydrodynamic forces to manipulate particles at a high inertia flow. In contrast to conventional microfluidics, where fluid inertia is negligible and flow is at the Stokes flow region ($\mathrm{Re} \ll 1$), the flow inertia is significant ($1 < \mathrm{Re} < 100$) and cannot be neglected for inertial microfluidics. The finite fluid inertia causes two intriguing effects: inertial migration and secondary flow. Inertial migration is a phenomenon where randomly dispersed particles migrate to a particular cross-sectional equilibrium position in a straight channel due to a hydrodynamic force, called the inertial lift force. This inertial lift force has two major components: shear gradient lift force and wall lift force. Shear gradient lift force arises due to the interaction of a particle with the background parabolic profile of the fluid velocity, and it tends to move the particle towards the channel walls. The wall lift force occurs due to the flow field interaction between particles and their nearby walls, repelling the particles away from the wall.[194] Based on the assumption that the particle is much smaller than the channel dimension, the net inertial lift force (F_L) can be expressed as:[195]

$$F_L = \frac{\rho_f U^2 d^4}{H^2} f_L(\mathrm{Re}, x) \quad (10)$$

where U is the average flow velocity, H is the hydraulic diameter, and f_L is the non-dimensional lift coefficient that is a function of the Reynolds number and the normalised cross-section position (x). Inertial microfluidic devices have been developed for particle manipulation and separation in the straight, serpentine, spiral, and contraction–expansion channels.[196–200]

The secondary flow is usually induced in a curved channel or a channel with disturbance obstacles, leveraging from the fluid momentum mismatch in the centre and near-wall region within the curvature or obstacle. The counterbalance of secondary flow drag (F_D) and inertial force (F_L) determines the final focusing positions and patterns of particles, Fig. 4(A). If $F_L \gg F_D$, particles will focus at the equilibrium positions due to the dominant inertial lift force. If F_L and F_D are in the same order, the original equilibrium positions will be modified due to the counterbalance of inertial lift force and secondary flow. If $F_L \ll F_D$, the secondary flow becomes dominant, and no focusing will be observed since the particles remain in the mixing streamlines.[194,201]

In a straight channel, inertial focusing of submicron to nanoparticles is challenging because the inertial lift force is too weak on the tiny particles. According to eqn (10), the inertial lift force is approximately 10^{-15}–10^{-13} N on 1 μm particles, and the efficient focusing of 1 μm particles requires an unpractical channel length of 1 m to 1 km. To overcome the channel length limitation, Mutlu *et al.*[179] proposed an oscillatory microfluidic device with a straight channel, Fig. 4(B). In this device, the flow direction is altered at a high frequency so that particles move back and forth, enabling an infinite axial movement within a fixed channel length. As flow velocity is symmetrical along the flow axis, the directionality of the inertial lift force acting on the particles is preserved despite switching of the flow direction. This technique demonstrates a successful inertial focusing of synthetic particles as small as 500 nm and a submicron bacterium, *Staphylococcus aureus*.

In a curved channel, the secondary flow is prone to retain the submicron/nanoparticles within the rotating streamlines because of a tiny inertial lift force. To confine the rotating streams of the secondary flow and suppress its mixing effect, shrunk asymmetric serpentine channels with smaller cross sections (width = 10–20 μm, height = 5–10 μm) were used to focus the submicron (200 nm, 600 nm, 920 nm and 2 μm) polystyrene spheres.[180] 2 μm and 920 nm particles were concentrated near the channel wall, while the 200 nm and 600 nm particles remained evenly distributed. Although inertial focusing of particles below 1 μm is challenging in a spiral channel, separating these particles was achieved using size-dependent movement trajectories of particles within a cross-sectional rotating stream.[182,202] Tay *et al.*[202] developed a high-resolution Dean flow fractionation (HiDFF) technique using a spiral channel to purify sub-micrometre particles. The device comprises two inlets separately for injecting the sheath flow and the sample. The transport distance varies with particle size during the Dean vortices-induced migration, Fig. 4(A). As a proof of concept, fractionation of drug-loaded particles for enhanced drug release and anti-tumour effects and isolation of circulating EVs from whole

blood using HiDFF were conducted. Recently, this technique was tailored to simultaneously separate exosomes, MVs and platelets from diluted whole blood for vascular risk profiling in type 2 diabetes mellitus (T2DM).[181] The team achieved a separation efficiency of 15 ± 3.8% for nanovesicles, which is three times better than UC.

The inertial microfluidic technology has the advantage of simplicity, high throughput, ease of operation, and good biocompatibility.[203–208] However, it is challenging to manipulate submicron and nanoscale particles because the inertial life forces are relatively weak and secondary flow is dominant. Moreover, this method lacks the capacity to further size-fractionated particles within submicron scales.

4.2 Deterministic lateral displacement

Deterministic lateral displacement (DLD) is a hydrodynamic-based microfluidic technique that uses tilted pillars to create unique flow streamlines and displace particles in predetermined paths according to their size.[209] Particles either follow a zigzag or bumping mode depending on their size, Fig. 4(C). The cut-off between these two modes is the critical diameter (D_c). Particles smaller than the critical diameter follow the initial streamline, defined as zigzag mode, whereas larger particles bump onto pillars and displace laterally to another streamline, termed as the bumping mode.[210] An empirical formula was derived for D_c by Davis *et al.*[211]

$$D_c = 1.4G\varepsilon^{0.48} \quad (11)$$

where G is the gap or pore size between the pillars. ε is the relative shift fraction that is the relative change in the position of the posts compared to the previous pillar row. The DLD technique is widely used for the separation of submicron to nanoparticles, including exosomes,[183] EVs,[184,185] bacteria,[212] synthetic beads,[213] and other biological particles.[214,215]

Wunsch *et al.*[183] developed a nano-DLD technology with a pillar gap of 235 nm to analyse, sort, and collect exosomes based on their sizes, Fig. 4(C). The nano-DLD array displaces larger exosomes (~100 nm) to the right side of the channel, whereas the smaller exosomes follow a zigzag or partial pumping mode and flow out of the array into the left outlet. However, the single array nano-DLD system has severe limitations in processing throughput. Therefore, the same group developed an integrated nano-DLD chip with 1024 parallel arrays interconnected by a fluidic bus network to enrich EVs from serum and urine.[184] Using pillar gaps of 225 nm, the team achieved an EV yield of approximately 50% for

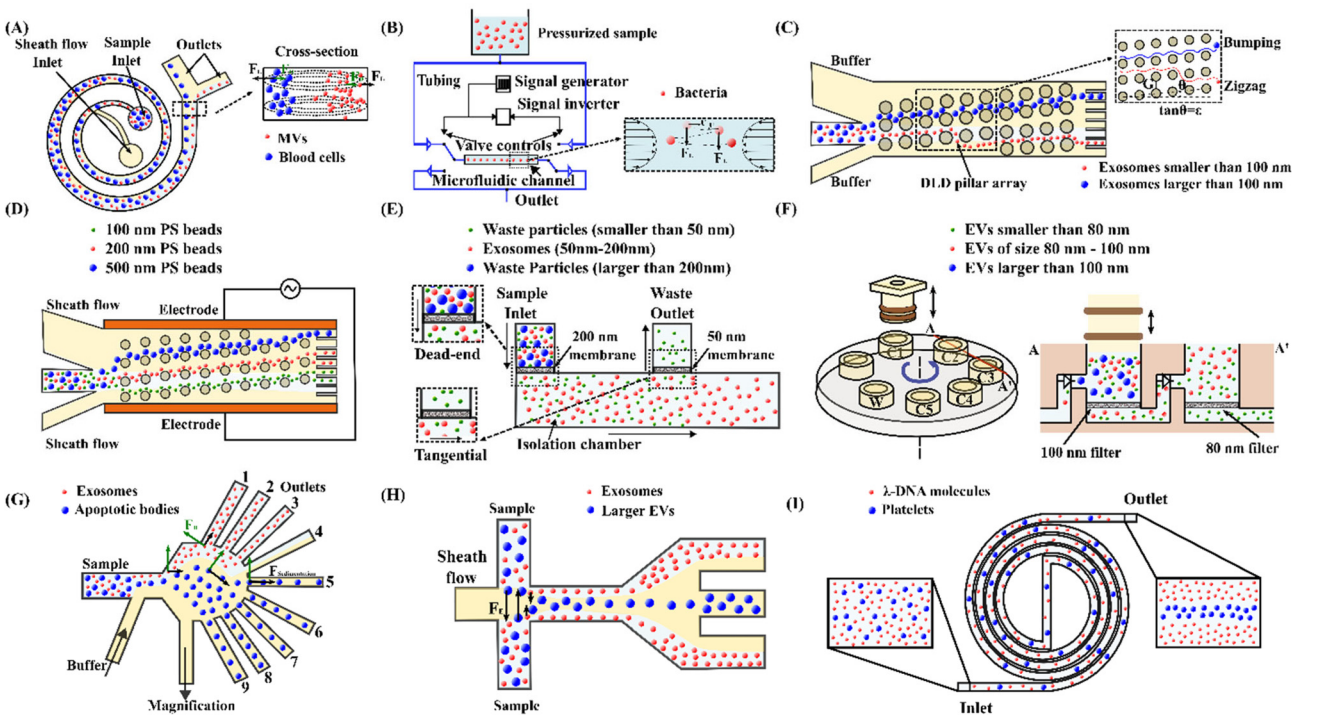

Fig. 4 Passive microfluidic techniques for manipulation, focus, and separation of submicron and nanoparticles. (A) High-resolution Dean flow fractionation of MVs in a spiral microchannel.[202] (B) Oscillatory microfluidic device for focusing bacteria.[179] (C) Separating exosomes based on their sizes using a DLD microfluidic device.[183] (D) Tuning of 100 nm, 200 nm and 500 nm polystyrene bead trajectories using an electrokinetic DLD microfluidic device.[216] (E) Integrated double-filtration microfluidic device for isolation of exosomes.[187] (F) Size-selective filtration of EVs with a movable plunger and rotational chip.[224] (G) Microfluidic PFF for separation of exosomes and apoptotic bodies.[189] (H) Isolation of exosomes from EVs by microfluidic viscoelastic flows.[193] (I) A double spiral microfluidic device for sorting of λ-DNA and blood platelets by viscoelastic microfluidics.[191]

both serum and urine. In addition to a high-pressure source, electroosmotic flow (EOF) was employed to drive fluids and particles into a nanopillar chip.[185] The design consists of four reservoirs to create EOF with electrical potentials. The flow velocity and direction can be easily controlled by adjusting the electric field applied to the reservoirs. The continuous fractionation of EVs was achieved in this device, where small vesicles of 50–400 nm and larger aggregates of more than 400 nm were collected in different reservoirs.

The critical diameter (D_c) is generally fixed for a DLD device with specific microstructure dimensions. To address this limitation, Gillams *et al.* demonstrated tuning of particle trajectories and deflected particles smaller than the D_c by incorporating an AC electric field orthogonal to the fluid flow in a DLD device, Fig. 4(D).[216] In the AC electric field, particles deflect due to nDEP force, making particles switch from zigzag to bumping mode. Without the electric field, polystyrene particles of 100 nm, 200 nm and 500 nm suspended in high conductivity electrolyte KCl showed a zigzag trajectory because they are significantly below the D_c (1–1.5 μm) of the device. In contrast, by applying 250 V_{PP} at 100 kHz frequency, 500 nm, 200 nm and 100 nm particles were deflected by 900 μm, 540 μm and 100 μm, respectively. Meanwhile, Zeming *et al.*[217] proposed a real-time D_c modulation using an electrostatic force. Various salt ionic concentrations created different thicknesses of the electric double layer, modulating the electrostatic force interactions between the nanoparticle and the pillar walls. In a low ionic concentration, particles experience an increasing lateral displacement, whereas the lateral displacement was lower for identical particles at a high ionic concentration. The team designed a DLD device with a pore size of 2 μm and a gradient space of pillar array, and the corresponding critical diameters ranged from 350 nm to 1000 nm in steps of 50 nm. The device could separate 51 nm and 190 nm fluorescent polystyrene beads in ultrapure DI water and 1000 nm and 1500 nm particles in 25 mM NaCl solution. In addition, to circular pillars, the same group studied the effects of pillar and particle shape and implemented an I-shaped pillar array for bacteria separation.[212] The team evaluated the performance of their devices using four species of bacteria. The experimental results indicated that the I-shaped design was the most effective for separating spherical and non-spherical particles.

The DLD technique can separate various particles with high resolution due to its simplicity, easy operation, and high precision. However, the limitations of DLD include low throughput, vulnerability to channel clogging, bulky setup and high fabrication cost.[210,218,219]

4.3 Microfluidic filtration

Microfluidic filtration employs porous membranes to separate particles by miniaturising ultrafiltration in a microfluidic platform. Particles smaller than the pore sizes pass through the membranes, while larger particles are trapped. There are two types of filtration strategies: dead-end and tangential flow. The sample moves perpendicularly to the membrane surface in the dead-end filtration. In contrast, the particles migrate parallelly along the membrane surface in the tangential flow filtration. This approach has successfully separated exosomes,[220] EVs,[120,221] viruses,[222] and nanoparticles.[223]

A tangential flow filtration device was developed to isolate and purify exosomes.[186] A nanoporous polycarbonate track etched (PCTE) membrane with a uniform pore size of 100 nm was stacked by two polymethyl methacrylate (PMMA) layers. Two identical serpentine channels were embedded in the top and bottom PMMA layers. The diluted plasma was injected into the top PMMA layer. The membrane trapped the exosomes while proteins and other small particles were washed out. The trapped exosomes were eluted by injecting DI water through a separate inlet. In a similar study, an enhanced microfluidic device was developed to isolate exosomes by combining dead-end and tangential flow filtrations, Fig. 4(E).[187] The sample was injected through the first 200 nm pore membrane as dead-end filtration to eliminate large debris. Next, a second 50 nm pore membrane trapped exosomes through a tangential flow strategy. A similar device was proposed by Liang *et al.*[188] to isolate EVs from urine, using a 200 nm and 30 nm pore membrane, respectively. The device retained and enriched exosomes with a 30–200 nm diameter at a 74.2% recovery rate. Another size-based exosome total isolation chip (ExoTIC) with a series of filter membranes of 200 nm, 100 nm, 80 nm and 50 nm pore sizes was developed to isolate EVs in specific size ranges.[220] Clinical samples passed through nanoporous membranes to enrich and purify intact EVs, but free nucleic acids, proteins, lipids and other small fragments were flushed out. This modular device successfully isolated EVs from clinical samples, including plasma, urine, and lavage, providing a 1000-fold yield compared to UC. A similar microfluidic device consisting of a vertically mobile plunger and a rotationally mobile chip was implemented for isolating EVs of multiple sizes, Fig. 4(F).[224] The rotational chip has five filtration chambers with nanopore filters with pore diameters of 200 nm, 100 nm, 50 nm and 30 nm, respectively. These chambers are sequentially connected *via* check valves that allow unidirectional flow when the plunger moves downward to push the fluids. Different chamber connections can separate EVs with various size intervals, and separated EVs can be collected from the respective chambers. Using Pluronic coating on the chamber surfaces to prevent nonspecific adsorption of EVs, the team obtained a high EV recovery rate of 89% from blood plasma.

Furthermore, Wang *et al.*[222] developed a disposable, pump-free, size exclusion-based filter microchip that can be used to separate viruses from unprocessed whole blood. An HIV-spiked whole blood sample was introduced to the microchip by pipetting. The filter membrane retained the blood components larger than the pore size, and a phosphate-buffered saline (PBS) solution was pipetted to

push the filtered virus to the outlet. The team was able to separate HIV with a recovery rate ranging from 74.2 ± 7.3% to 84.3 ± 4.7% using a 1 μm pore size filter and 73.1 ± 8.3% to 82.5 ± 4.1% using a 2 μm pore size filter.

Microfluidic filtration is a simple, label-free, and flexible method.[225] The cut-off size can be easily controlled by membrane pore size. However, like ultrafiltration, the trapped particles can accumulate on the membrane, causing clogging and fouling issues.[226] Furthermore, biological particles may be exposed to shear stresses when squeezed through filter pores. The shear stress may negatively impact the biological integrity of filtered particles.[227]

4.4 Pinched flow fractionation

Pinched flow fractionation (PFF) employs pinching particles with hydrodynamic flows and separating them according to their size. PFF devices consist of two inlets for sample and secondary flows, a contraction that works as the pinched section, an expansion section and multiple outlets. A secondary flow continuously pinches all particles suspended in a fluid toward the sidewall.[228] Smaller particles stay closer to the wall compared to the larger particles. In the expansion section, the lateral difference of differently-sized particles is amplified due to the expanding fluid streamlines, enabling size-based separation of various particles *via* multiple outlets.[229] PFF has been employed for the isolation of synthetic and biological nanoparticles.[189,190,230–232]

Controlling the distribution of the fluid streamline is critical for the sorting of particles in PFF. A PFF device with a magnification channel was reported for non-invasive size-based EV separation.[189] In the device, a magnification channel draws partial flow before the expansion section, which helps to alter the streamline separation and vesicle allocation to the outlets, Fig. 4(G). This work defined a magnification ratio as the flow rate ratio in the magnification channel to the total flow rate. The introduction of the magnification channel achieved increased efficiency at minimum sample dilution. A magnification ratio of 75% allowed the authors to observe exosomes at outlets 1 to 3 and apoptotic bodies at outlets 5 to 9. Exosomes with cup-shaped morphology of 30–100 nm were collected at outlet 2, whereas aggregates with sizes of 500 to 2000 nm were gathered at outlet 8. Meanwhile, Hamacher *et al.*[233] developed a microfluidic chip based on PFF to separate spermatozoa from virus-spiked semen. With the optimised flow rate ratios (total flow/sample flow) of 24–32 and fluid removal fraction (percentage of flow to waste outlet) of 2.7%, they recovered 86 ± 6% of spermatozoa and removed 84 ± 4% of cowpea chlorotic mottle virus (CCMV). This technology may help reduce the spread of disease in the context of artificial insemination in the veterinary industry.

Furthermore, another study employed a polydimethylsiloxane (PDMS) membrane microvalve at one outlet to tune the effluent position of the particles.[190] The microfluidic device comprised outlet 1 with the microvalve and four other valveless outlets. Flow rate tuning at the corresponding outlet was achieved by controlling the microvalve using positive pneumatic pressure. When the microvalve was partially closed, the flow rate at outlet 1 was reduced, allowing the larger particles to shift away from outlet 1, while the effluent position of smaller particles remained unchanged. Initially, fluorescent polystyrene beads with diameters of 0.5 μm and 0.86 μm both exited through outlet 1 without actuation of the microvalve. But after applying 18.0 kPa to the microvalve, 0.5 μm and 0.86 μm particles were separated successfully, with a purity of 90% at outlet 1 for 0.5 μm particles and 82% at outlet 2 for 0.86 μm particles.

PFF is excellent for isolating particles of various sizes due to its simple design and convenient fabrication processes. However, this technique provides low throughput and low efficiency compared to the other hydrodynamic-based separation techniques.[234,235] The substantial sample dilution is another significant drawback of this technique.

4.5 Viscoelastic microfluidics

Viscoelastic microfluidics manipulates particles using elastic effects of a non-Newtonian medium.[236] An elastic force arises due to the imbalance of normal stresses in viscoelastic fluid flow. Both the first normal stress difference ($N_1 = \tau_{xx} - \tau_{yy}$) and the second normal stress difference ($N_2 = \tau_{yy} - \tau_{zz}$) contribute to the elastic force. τ_{xx}, τ_{yy} and τ_{zz} are the normal stresses in streamwise, transverse, and vorticity directions, respectively.[237–239] In a diluted viscoelastic solution, N_2 is negligible as its magnitude is significantly lower than N_1.[240] Therefore, the elastic lift force (F_E) is proportional to the variation of N_1 over the particle size and can be expressed as:[241]

$$F_E = C_{eL} d^3 \nabla N_1 = -2 C_{eL} d^3 \eta_p \lambda \nabla \dot{\gamma}^2 \quad (12)$$

where C_{eL} is the non-dimensional elastic lift coefficient, η_p is the polymeric contribution to the solution viscosity, λ is the relaxation time, and $\dot{\gamma}$ is the average shear rate. The combination of the inertial and elastic effects determines the focusing regions of particles in the microchannel.[242–244] In viscoelastic fluids, particles migrate to the centre of the channel under the elasto-inertial effect, and the migration speed is proportional to particle size. This size-dependent lateral migration speed creates a lateral gap between various particles. These phenomena have been used in a wide range of particle manipulation and separation applications.[191,192,245–247]

Kim *et al.*[192] firstly discovered that submicron colloidal particles (500, 200 and 100 nm in diameter) and macromolecules (λ-DNA and T4-DNA with radii of gyration of ~0.69 and 1.5 μm, respectively) could be focused decently in a viscoelastic fluid flow. The discovery indicated the potential of viscoelastic microfluidics for submicron particle manipulation. Since then, this technique has attracted

increasing attention for submicron particle focusing and separation.[193,246,248–250] For instance, Liu *et al.*[193] proposed a viscoelastic microfluidic device for the size-based separation of exosomes from larger EVs. The device consists of a straight main channel, two inlets for the sample and sheath flow, and three outlets, Fig. 4(H). Both sample and sheath flow contain a low concentration of polyethylene oxide (PEO), so that the elastic lift force exerted on the nanoparticles controls their lateral migration. Larger EVs migrate faster to the centre of the microchannel and are collected from the middle outlets, whereas exosomes moving very slowly are collected at the side outlets. Later, the team employed a modified viscoelastic medium by dissolving λ-DNA in Tris–borate–EDTA (TBE) buffer as the central sample flow and a Newtonian TBE buffer for the sheath flow. They applied the modified viscoelastic microfluidic device to fractionate EV subpopulations, *i.e.*, exosomes, MVs, and apoptotic bodies.[246] Nam *et al.*[248] reported a sheathless viscoelastic microfluidic device to isolate submicrometer platelet-derived microparticles (PDMPs) from whole blood. Since the diameters of RBCs and platelets are significantly higher than the diameter of PDMPs, they can be concentrated at the channel centre and filtered out from the middle outlet. In contrast, PDMPs are uniformly distributed and partially extracted from the side outlets.

Apart from straight channels, spiral and wavy channels have also been explored for viscoelastic manipulation of submicron and nanoparticles. A double spiral microchannel has been developed to manipulate synthetic nanoparticles and λ-DNA molecules, Fig. 4(I).[191] In this geometry, the smaller particles (49, 100, 500 and 1000 nm in diameter) were focused along the channel centre. In contrast, the larger particles (2000 nm in diameter) focused off the centre near the two side walls. The device demonstrated high-quality sorting of a binary mixture of nanoparticles. Both polystyrene particles (100/2000 nm) and λ-DNA/blood platelet mixtures were sorted with separation efficiencies above 95%. Recently, a spiral channel device was applied to separate U87 glioblastoma cell-derived small and medium size EVs. In this work, medium EVs (mEVs) could be focused, but sEVs were too small to be focused and randomly dispersed.[250] They recovered 55% of sEVs with 6% contamination of mEVs and 80% of mEVs with 22% contamination of sEVs after one round of recycling.

Furthermore, a wavy microchannel was developed for submicron particle focusing and exosome sorting using viscoelastic fluids.[249] Besides the elastic lift force, the wavy channel induces an additional Dean flow, facilitating effective focusing of particles towards the channel centre. Large particles (300, 500 and 1000 nm) were effectively focused, whereas small particles (100 nm) were kept widely distributed at the end of the channel. After applying a sheath flow to pinch all particles along the sidewalls at the inlet, the device was used to sort exosomes from large EVs based on the size-dependent migration speed.

Viscoelastic microfluidics is a promising technique for manipulating submicron particles. This technique is label-free, simple, and biocompatible.[49] It has a much higher separation resolution (~O(100 nm)) than inertial microfluidics (~O(1 μm)), since the elastic lift force is at least one order of magnitude higher than that of the inertial lift force for submicron particles.[193] In addition, viscoelastic microfluidics uses relatively larger channel space than DLD and microfiltration, lessening channel blockage issues and fabrication costs. One limitation is the need for specialised viscoelastic medium preparation. The elasticity enhancers may contaminate biological samples, and the enhanced viscosity may require a higher pressure drop to drive the sample.[238] Moreover, the throughput is still low compared to the conventional techniques. Finally, manipulating nanoscale particles is still a major challenge and has been less explored.[191]

5 Hybrid microfluidic techniques

Hybrid microfluidic techniques integrate two or more techniques discussed above in a serially connected or physically coupled manner.[33] Hybrid microfluidics can combine the advantages of each method and potentially overcome the limitations of individual ones through the synergy of inherent characteristics. Therefore, superior performance and more versatility are expected. However, due to the complexity of the integration, physical coupling and device design, very few studies have been reported on manipulating submicron and nanoparticles using hybrid microfluidic techniques.

5.1 DEP–MP

Integrating DEP and magnetophoresis in a single microfluidic device achieved high-purity sorting of multiple bacterial targets.[251] The integrated dielectrophoretic–magnetic activated cell sorter (iDMACS) consists of a dielectrophoretic separation module and a serial magnetic separation module, Fig. 5(A). Three distinct bacterial clones of an *E. coli* strain were labelled with DEP, magnetic and no tags. In the DEP separation module, the bacteria strain labelled with DEP tags was efficiently deflected from other bacteria and eluted from the upper outlet. In contrast, the magnetic tagged and non-tagged strains were retained in the fluid streamline and entered into the downstream magnetic separation module. In the magnetic separation module, the external magnetic field activated the titanium/nickel structure and captured the magnetically tagged bacteria, whereas non-tagged bacteria continuously passed through. After the entire sample was processed, the magnetic tagged bacteria strain was retrieved by removing the external magnetic field. Target bacteria strains with DEP and magnetic tags achieved a separation purity of 98.6% and 95.6%, respectively, without cross-contamination between targeted strains. The waste fraction consisted mainly of non-tagged cells (99.74%), and the de-labelling of tagged bacteria during the separation process probably contributed to the slight contamination.

5.2 AP–DEP

A virtual DLD (vDLD) microfluidic device was developed by integrating acoustic and DEP forces, Fig. 5(B).[252] An array of IDTs on a piezoelectric lithium niobate substrate can generate both acoustic and electric force fields. Acoustic forces allow for isolating particles based on mechanical properties such as compressibility and density, whereas DEP can sort particles based on electrical properties such as permittivity. Either of these forces can be employed for the separation of particles. By tuning the strength of the dominant force, larger particles are captured in the force field and deflected laterally, while smaller particles are not affected. The device demonstrated the separation of 500 nm particles from 300 nm particles with an efficiency of 87%. Later, the vDLD device was modified to sort exosomes and MVs, taking advantage of combined acoustic and DEP forces with tilted-angle IDTs.[253] In this device, the cut-off size of particles for separation (or critical diameter) was determined by coupling acoustic radiation, DEP and fluid drag forces. The concurrent acoustic and DEP forces significantly reduced the critical diameter while doubling the lateral displacement of particles compared to the previous version. The combined acoustic/electric approach achieved exosome isolation of more than 95% purity and 81% recovery.

6 Nanoparticle detection techniques after separation

Due to the vast utilisation of nanoparticles, more precise and reproducible characterisation techniques are also required after separation. Various nanoparticle detection techniques have been developed based on their inherent physical and chemical properties. Here, we mainly discuss the seven most common methods: electron microscopy, dynamic light scattering, nanoparticle tracking analysis, atomic force microscopy, fluorescence analysis, colourimetric detection, and electrochemical detection.

6.1 Electron microscopy

Compared with the traditional optical microscopy, electron microscopy (EM) uses electrons as the source of illuminating radiation instead of visible light to obtain sample images, Fig. 6(A). The shorter wavelength of the electron beam overcomes visible light's resolution limitation, which renders higher resolution up to 1–5 nm. This technique has emerged as a powerful tool for characterising a wide range of biological and non-biological particles.[255] Typically, according to the different imaging mechanisms, EM can be divided into two main types: transmission electron microscopy (TEM) and scanning electron microscopy (SEM). TEM uses a high-energy electron beam transmitted through the specimen to obtain a projection image. Meanwhile, the electron diffraction pattern gained by transmitted electrons resulted in Bragg scattering which provides crystal structure information of the samples. Therefore, TEM would be an ideal technology for metal or crystal particle identification and analysis. Under specific sample preparation processes, TEM can also be utilised to analyse nanoparticle size and shape, providing the most accurate estimations of nanoparticle homogeneity for applications such as cell biology.[256] In contrast, SEM works by scanning the surface of an object with a focused beam of electrons and images the sample by collecting electrons reflected from or knocked off the sample surface, Fig. 6(A).[257] As a result, SEM can acquire clear 3D morphology with a depth of field and information about the sample's surface and composition.[258–260] In addition, SEM can operate in transmission mode, known as transmission scanning electron microscopy (TSEM). It has shown immense potential in the accurate measurement of dimensions of nanoparticles.[261] Although the extremely high resolution of TEM and SEM advances the characterisation of particles, the complicated sample preparation procedures (dehydration, conductive treatment, thinning) and harsh testing requirements (high vacuum, high-energy electron beam) make it complicated to get *in situ* results, and may also cause damage to the subtle samples. Approaches like cryo-electron microscopy have been implemented to avoid the effects of the aforementioned drawbacks. EM is not an excellent choice for real-time and non-invasive particle measurement.

6.2 Dynamic light scattering

Dynamic light scattering (DLS) is commonly used to measure the size of nanoparticles suspended in a liquid with a laser beam passing through the bulk sample. A photodetector is usually positioned at an angle with the incident light to

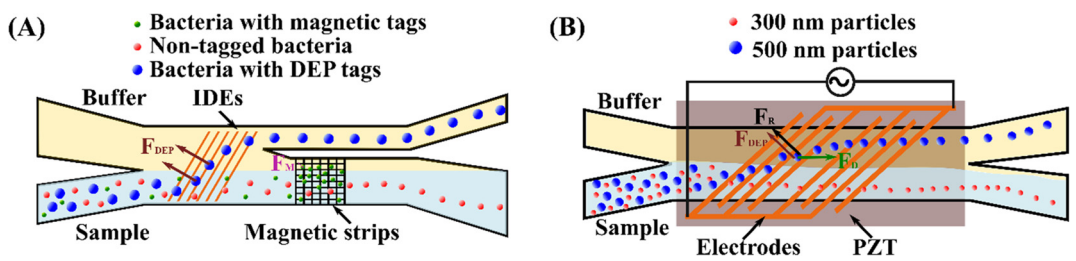

Fig. 5 Hybrid microfluidic techniques for sorting submicron and nanoparticles. (A) Sorting multiple bacterial targets by serially combining DEP and MP in an integrated DEP–MP cell sorter.[251] (B) A vDLD system for sorting sub-micrometre particles by coupling acoustic and DEP forces.[252]

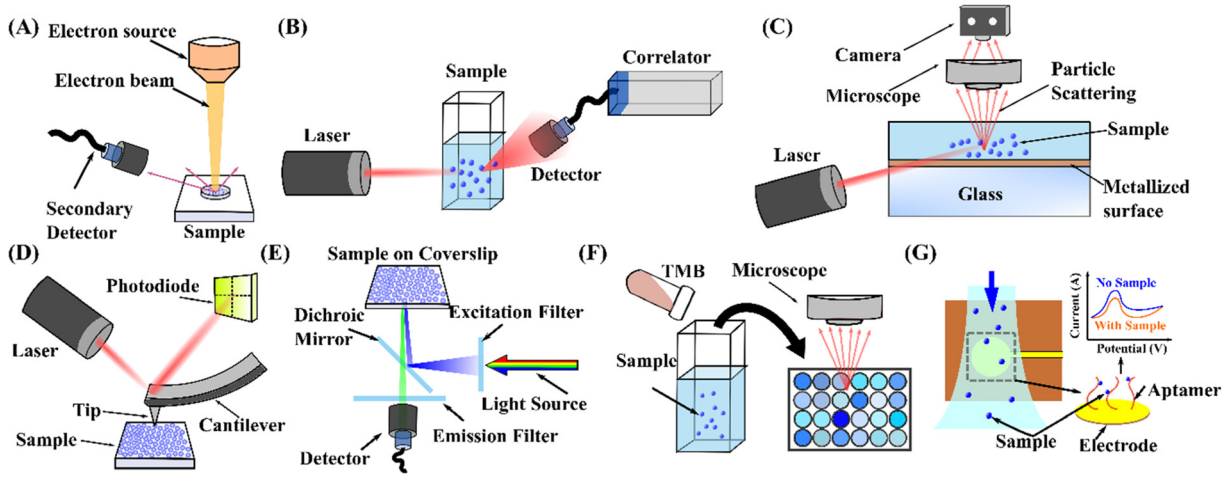

Fig. 6 Schematic representation of the working principle of nanoparticle measurement and detection techniques. (A) Electron microscopy.[260] (B) DLS.[265] (C) NTA.[267] (D) AFM.[279] (E) Fluorescence detection.[286] (F) Colourimetric detection.[294] (G) Electrochemical detection.[304]

collect the scattered light intensity from the particles, Fig. 6(B). The fluctuation of the scattered light due to the Brownian motion of particles correlates with their velocity. An autocorrelator estimates the diffusion coefficient and the hydrodynamic radius using the Stokes–Einstein relationship.[262] DLS is a non-invasive, highly reproducible, time-efficient, and low labour-intensity technique for characterising nanoparticles.[263] However, due to the difficulty of extracting specific particle size information from the autocorrelation function, DLS cannot distinguish between polydispersed particles of a similar size range and becomes less reliable when measuring samples with broad particle size distribution.[264] In addition, as the obtained decay rate of the correlation from the initial state is an average value, the distribution data acquired from DLS may not be reliable. The particle aggregation may also result in more significant measurement errors.[265] Nonetheless, the high sensitivity of DLS can be utilised for disease diagnosis, such as rapid screening of virus–antibody binding by detecting the formation of virus–antibody aggregates.[266]

6.3 Nanoparticle tracking analysis

Nanoparticle tracking analysis (NTA) utilises light scattering to acquire the size, distribution and concentration of nanoparticles in a dispersed medium.[264] In contrast to DLS, NTA technology is equipped with a charge-coupled device (CCD) or complementary metal oxide semiconductor (CMOS) sensor camera to enable the activity processing of particles, estimating their speed due to Brownian motion, Fig. 6(C).[267] Therefore, the hydrodynamic diameter of a particle can be evaluated by the Stokes–Einstein equation.[268] NTA provides information on the size distribution and concentrations of monodisperse and polydisperse particle samples and can also be employed to differentiate single nanoparticles based on their reflective index.[269,270] Furthermore, NTA offers greater flexibility and robustness in characterising biological nanoparticles and importantly, it is not biased towards larger nanoparticles or aggregates compared to other measurement techniques.[271–273] Nevertheless, NTA is time-consuming and requires expert operational skills to conduct the measurements.[269] Moreover, a large particle in the solution, such as debris or impurities, will scatter at high intensity and introduce significant errors in the analysis. Furthermore, since the measuring chip of the fluid channel only contains a small volume, repetitive measurements should be carried out to obtain reliable results.

6.4 Atomic force microscopy

Atomic force microscopy (AFM) provides high spatial resolution in nanoparticle measurements.[274] A tiny sharp tip connected to an ultra-small force-sensitive cantilever is used as the probe for x–y grid scanning the samples by direct contact with the sample surface. A laser beam detects and measures the deflection of the cantilever in AFM, Fig. 6(D).[267] Therefore, AFM can simultaneously measure the size distribution and mechanical properties such as friction, energy dissipation, tension, pressure, and reversible and irreversible deformation.[275–277] Since the operating procedure does not require specific sample preparation and measurement environment, AFM can also characterise biological samples in liquids, such as those found under physiological conditions.[278] Due to these superior capabilities, AFM has the potential to be used as a diagnostic tool for cancer. For instance, the changes in ultrastructure and mechanical properties within tumour tissues and cells can be employed as a marker for clinical diagnostics.[279] However, AFM measurement of soft matter shows errors in height due to tip pressing and lateral size due to tip-broadening effects. To overcome this drawback, a tapping mode has been utilised to measure soft matter.[280] A constant amplified oscillation was applied to the cantilever during the tapping mode. The piezo signal varies when the tip comes

close to the surface, enabling the morphology scanning of samples such as proteins and exosomes. Meanwhile, a novel image reconstruction algorithm has also been developed for high-speed AFM known as localisation AFM (LAFM), allowing the extraction of high-resolution information in the study of single biomolecules beyond the tip radius resolution limit.[281] Moreover, the scanning measurement mechanism allows AFM to obtain accurate size distribution information of the polydisperse system, which is not applicable in DLS.[282] Nevertheless, bubbles or droplets of similar size and shape in the sample can interfere with particle classification. Therefore, combining the characterisation results with other techniques is encouraged for better results.

6.5 Fluorescence detection

Fluorescence imaging technology is adapted for detecting nanoparticles in microfluidics due to its accuracy and sensitivity.[227] Fluorescence is the emission of light from a substance that has absorbed light or other electromagnetic radiation. Its intensity, wavelength and luminescence time depend on fluorophore material properties. Fluorescent molecules are used to tag biological particles to facilitate detection in microfluidic channels with the aid of fluorescence emission parameters.[138,283] Fluorescence imaging has shown good accuracy and high sensitivity in exosome detection. Exosomes labelled with fluorescent dyes can be quantified using standard plate readers by measuring the fluorescence intensities at excitation and emission wavelengths, Fig. 6(E).[284] In addition, immunofluorescently stained exosomes can be characterised and quantified using an inverted fluorescent microscope.[285] This technique provides the highest spatial resolution for disease diagnosis at the microscopic level.[286] Due to its unique advantages, it has been employed for various chemical and biological applications.[287,288] However, prolonged exposure to fluorescent light can result in loss of intensity, affecting the accuracy of the detection results.[289]

6.6 Colourimetric detection

Colourimetric detection allows direct visualisation of samples to detect nanoparticles. This method works by comparing or measuring the colour depth of chromogenic substances. 3,3′,5,5′-Tetramethylbenzidine (TMB) is widely used as a chromogenic substance for exosome detection due to its high sensitivity and high colour purity.[290,291] The oxidation of TMB provides the ability to obtain naked eye read-outs by converting a colourless solution to blue colour.[292] The absorbance change is directly proportional to the concentration of target particles so that captured particles can be quantitively determined, Fig. 6(F).[293] Recently, microfluidic technology has been combined with colourimetric detection to visualise exosomes and EVs.[221,294] Furthermore, this detection technique enables cost-effective and straightforward monitoring of heavy metal ions associated with environmental pollution and health-related risks.[295] Nevertheless, it is less sensitive and requires higher sample concentration.[296,297] Moreover, colourimetric detection exhibits constraints in determining individual components from a mixture.[298]

6.7 Electrochemical detection

The electrochemical detection technique detects electrical signal changes between electrodes by a target-induced chemical reaction.[299] Due to chemical or biochemical reactions, electrical properties around electrodes can vary, and changes in the electrical signal, such as current, can be detected. With the maturity of micromachining technologies, the integrated microelectrodes implemented on microfluidic platforms have enabled the detection of biomolecules with high sensitivity.[300–302] For instance, electrodes modified with a CD63-specific aptamer have been developed to capture exosomes and emit an electrochemical signal for quantification.[8,303,304] Electrochemical detection has many advantages, such as reduced reagent requirements, high sensitivity, low cost, and rapid detection.[305–307] Besides, it is independent of the optical path length and sample turbidity.[308] However, the inability to detect non-electroactive nanoparticles and the need for solutions with strong acidic or oxidant characters prevent colourimetric detection from being a universal detection technique.[309]

7 Discussion and perspectives

This paper studied the conventional and microfluidic technologies for the manipulation and separation of submicron and nanoparticles. We discussed the principle of five standard traditional techniques: ultracentrifugation, ultrafiltration, size exclusion chromatography, precipitation and immunoaffinity capture. We subsequently classified the microfluidic technologies as active, passive and hybrid technologies based on the sources of the main manipulating forces. We elaborated on the physics of manipulating forces and the working mechanism of reported devices and discussed the features, limitations and applications of these techniques. Table 1 summarises and compares the principles, applicable particle sizes, particle types, separation efficiencies and throughput, as well as the merits and demerits of both conventional and microfluidic techniques. The conventional techniques generally possess the advantages of time efficiency, high yield, ease of use and good reproducibility, but they are limited by the high cost and low purity. Microfluidic technologies, which can manipulate fluid flow and particles precisely in a microscale space, are promising alternatives to provide complementary capacity for enhanced separation resolution. Although significant progress has been achieved in microfluidic technology with a broad range of applications, there is still a considerable gap to be filled to enable microfluidic technology to be as mature as conventional technologies.

The major challenge associated with the effective manipulation and separation of submicron and nanoparticles

is the minuscule size of the particles. Both the active and passive manipulating forces are proportional to a higher order of particles size ($F \sim a^n$; $n > 1$, *e.g.*, $n = 3$ for dielectrophoresis, magnetophoresis, and viscoelastic forces) than the fluidic drag force ($F \sim a$), and the size reduction of particles toward the nanoscale sharply decreases the manipulating forces. Moreover, the manipulating forces drop much faster than the drag force when reducing the particle size. In contrast, Brownian motion becomes more significant for nanoparticles, negatively impacting the effective manipulation of nanoparticles. To address these issues, possible solutions may arise from the following perspectives: (i) the amplification of the overall size of target nanoparticles; (ii) the enlargement of local physical strength and gradient; and (iii) the combination of multiple manipulating forces. One way to amplify the overall size of target nanoparticles is by binding the nanoparticles specifically with larger microscale beads. Target nanoparticles can be tagged to microbeads of distinct sizes. Subsequently, the manipulating force will be scaled up as on microparticles, and the size difference of nanoparticles in the nanoscale can be translated into the difference in microscale, significantly lessening the technical challenges of separation. A successful example was reported by Sarkar *et al.*,[310] who used microbeads of different sizes to selectively bind multiple proteins and separate these microbeads successfully using an inertial microfluidic device. Therefore, the various proteins can be divided in a continuous manner. Another microscale approach is to induce the self-aggregation of target nanoparticles using methods such as precipitation. This method also results in a larger cluster of nanoparticles, but the co-precipitation of non-target particles should be avoided.

Enlarging the local physical strength and its gradient is another feasible method to amplify manipulating forces, because manipulating forces are based on electric and magnetic fields and depend not only on the strength of these physical fields but also on their gradients, as shown in eqn (4) and (9). Apart from applying a high electrical or magnetic field, well-defined microscale structures (*e.g.*, insulating microposts,[132] microelectrodes,[134,135] and magnetic micropole arrays[146]) with microscale nonuniformity close to the manipulation region can induce high physical gradients. Therefore, the resulting forces are sufficient to manipulate nanoscale particles. Furthermore, combining multiple manipulating forces is also a strongly feasible approach. Although a single manipulating force is not strong enough or not sensitive enough to distinguish nanoparticle populations, adding up multiple forces on a mixture of nanoparticles could enhance the manipulation capacity. The design of multiple physical coupling is challenging, and only one successful work has been reported thus far. Ai's group has developed a novel microfluidic device combining acoustic and DEP forces to sort exosomes and MVs.[253] In their work, coupling acoustic with DEP forces resulted in a much larger net force to counterbalance the mainstream drag force, enabling an effective manipulation of nanoparticles with a significantly reduced size. Besides, a more significant lateral net force allowed an enhanced deflection of particles, magnifying the lateral displacement of particles. The combined acoustic/electric technology improved exosome isolation in purity and recovery. A precise design of each manipulating physical force and how they are coupled is critical to ensure the successful coupling of multiple physics. More efforts are needed in the future to explore different coupling schemes of various forces. Another way to combine various force fields is to connect several manipulating sections consecutively. In each section, a manipulating force field dominates the isolation of particles based on the local selection criterium. Multistage processing, passing through several consecutive stages, is expected to promote separation purity and enhance the versatility of devices in the fractionation of complex samples. For consecutive connection, the adjacent stages are linked by the fluid flow, and the flow rate of the outlet upstream must match the inlet of the second stage. The flow speed needs to be tuned to meet the operating flow range for upstream and downstream stages. One way is to modify the channel cross-sectional area at different sections to optimise the linear flow speed. The other way is to exhaust partial fluids upstream or supplement additional fluid to lower or enhance the downstream flow speed. In addition, a pumping unit between the connective units can adjust the flow speed for the second stage. In this case, a large reservoir may collect and store the outlet sample from the first stage.[33]

For passive microfluidic technologies, the channels or gap spaces were generally scaled down to submicron and even nanoscale to adapt to the nanoparticles.[180,183] However, minuscule fluidic channels and gap spaces inevitably bring about a very high fluidic resistance, and thus, a powerful pumping system is needed to drive the sample into the device. Moreover, the high bonding strength of device layers is required to prevent delamination, and a more robust assembly connecting tubing to the microfluidic device input ports is also necessary. Furthermore, a deformation of the microchannel may become more significant under high pressure, which may impair the functionality of the device. These all add to the technical challenges of microfluidic technology for processing nanoparticles. Therefore, device materials, fabrication, assembling, and pumping are critical in designing microfluidics for nanoscale particles.

The miniaturisation of conventional techniques into a microfluidic platform can reduce reagent consumption and sample volume. Due to the significant advantages of precisely controlling fluid flow in microfluidics, controlling fluid motion and the procedure of multiple fluids to filtrate multiple components becomes feasible. The miniaturisation of ultrafiltration successfully formed microfluidic filtration by embedding membranes into microfluidic channels.[311] The nanoparticles can be controlled to move at different orientations toward the membranes and at multiple stages to achieve the versatility of the devices. More recent work

reported the miniaturisation of size exclusion chromatography (SEC) in microfluidics.[312] Benefiting from the precise control of fluid flow in microfluidics, the authors successfully regulated the hydraulic resistances in a T-junction channel to address the significant challenge of on-chip sample injection. Combining precipitation with microfluidics is also promising but not fully explored. Microfluidic devices can potentially be utilised to control the mixing of precipitation agents and samples. In addition, microfluidic devices can continuously remove the precipitated target particles from the suspension without requiring centrifugation or filtration.

Microfluidics can miniaturise conventional techniques to improve the separation resolution. It also has the benefit of handling samples of small volumes. However, a larger sample volume is required for some applications, such as isolation of exosomes for therapeutic purposes[313] or treatment of the environment and industry nanoparticles.[314,315] The throughput of microfluidic technologies needs to be scaled up to reach or even exceed the level of conventional technologies in fulfilling these tasks. Parallelisation of microfluidic channels is a possible way forward, and careful design and optimisation are necessitated to ensure uniformity between multiple channels. For passive microfluidic techniques, the devices work only by channel geometry or hydrodynamic forces. For the microchannels with one inlet, scaling up the throughput can be readily achieved by patterning multiple functional channels along the horizontal, radial, and vertical directions.[316–319] However, more efforts should be made to the microchannels with two or more inlets to ensure fluid flow consistency between parallel channels. Moreover, upscaling the design for active microfluidic devices is more challenging. Active microfluidic techniques use external acoustic, electric, magnetic and optical force fields to manipulate particles. Consistency in fluid flow and external force fields between multiple parallel channels demands a delicate design. In addition to an elevated throughput, a parallelisation of channels can also reduce the overall fluidic resistance since the net channel cross-sectional area is amplified by the number of parallel channels and the fluidic resistance is reversed to the channel cross-sectional area.

In conclusion, microfluidic technologies have distinct advantages and benefits compared to conventional techniques regarding separation resolution and purity. Although significant progress has been achieved in microfluidic submicron and nanoparticle manipulation, it is still in its early development stage. A broad field region is still not explored and exploited in the aspects of the fundamental mechanism, device design and applications. Besides the manipulation and separation, integrating other functional units, such as mixing, synthesis, counting, detection, and analysis, into one microfluidic platform is an excellent prospect for novel automated and portable solutions. To elevate microfluidic technologies to the maturity of conventional methods, further significant efforts are urgently needed to tackle the current limitations on throughput, manipulating accuracy, separation resolution, device material, and connection strength.

Lists of abbreviations

EVs	Extracellular vesicles
MVs	Microvesicles
DEP	Dielectrophoresis
FFF	Field flow fractionation
DLD	Deterministic lateral displacement
PFF	Pinched flow fractionation
AP–DEP	Acoustic–dielectrophoresis
DEP–MP	Dielectrophoretic mangenetophoresis
AFM	Atomic force microscopy
NTA	Nanoparticle tracking analysis
DLS	Dynamic light scattering
UC	Ultracentrifugation
DGUC	Density gradient ultracentrifugation
UF	Ultrafiltration
SEC	Size exclusion chromatography
AP	Acoustophoresis
SAW	Surface acoustic wave
BAW	Bulk acoustic wave
IDT	Interdigitated transducer
SSAW	Standing surface acoustic wave
TSAW	Travelling surface acoustic wave
RBC	Red blood cell
WBC	White blood cell
CP	Capillary electrophoresis
GE	Gel electrophoresis
DC	Direct current
ELDS	Evaporative light scattering detector
AC	Alternating current
CM	Clausius–Mossotti
DC-iDEP	Direct current insulator-based dielectrophoresis
ACE	Alternating current electrokinetics
DENV	Dengue virus
4G2	Mouse anti-flavivirus monoclonal antibody
MP	Magnetophoresis
SPLITT	Split-flow lateral-transport thin
HiDFF	High-resolution Dean flow fractionation
T2DM	Type 2 diabetes mellitus
EOF	Electroosmotic flow
PCTE	Polycarbonate track etched
PMMA	Polymethyl methacrylate
ExoTIC	Exosome total isolation chip
PBS	Phosphate-buffered saline
CCMV	Cowpea chlorotic mottle virus
PDMS	Polydimethylsiloxane
PEO	Polyethylene oxide
TBE	Tris–borate–EDTA
PDMP	Platelet-derived microparticles
sEV	Small extracellular vesicle
mEV	Medium extracellular vesicle

iDMACS	Integrated dielectrophoretic–magnetic activated cell sorter
vDLD	Virtual deterministic lateral displacement
EM	Electron microscopy
TEM	Transmission electron microscopy
SEM	Scanning electron microscopy
3D	Three dimensional
TSEM	Transmission scanning electron microscopy
CCD	Charge-coupled device
CMOS	Complementary metal oxide semiconductor
LAFM	Localisation atomic force microscopy
TMB	3,3′,5,5′-Tetramethylbenzidine

Author contributions

J. Z. and N. T. N. conceived the idea and designed and supervised the project. S. H. conducted the literature study, drew the figures, and wrote the manuscript. J. Z. contributed to the discussion and perspectives. H. C. and A. M. contributed to drawing the figs. L. O. contributed to the measurement and detection techniques. J. Z., N. T. N., H. A., G. K., and N. K. revised and modified the manuscript. All the authors provided critical feedback and read and approved the manuscript.

Conflicts of interest

The authors have declared no conflict of interest.

Acknowledgements

The authors acknowledge the support from the Australian Research Council (ARC) Discovery Project (Grant No. DP180100055), ARC DECRA fellowship (Grant No. DE210100692) and ARC Future Fellowships (FT180100361).

References

1 C. M. Abreu, B. Costa-Silva, R. L. Reis, S. C. Kundu and D. Caballero, *Lab Chip*, 2022, **22**, 1093–1125.
2 J.-J. Lee, K. J. Jeong, M. Hashimoto, A. H. Kwon, A. Rwei, S. A. Shankarappa, J. H. Tsui and D. S. Kohane, *Nano Lett.*, 2014, **14**, 1–5.
3 T. Hamacher, J. T. W. Berendsen, J. E. van Dongen, R. M. van der Hee, J. J. L. M. Cornelissen, M. L. W. J. Broekhuijse and L. I. Segerink, *Lab Chip*, 2021, **21**, 4477–4486.
4 M. Bouri, R. Salghi, M. Algarra, M. Zougagh and A. Ríos, *RSC Adv.*, 2015, **5**, 16672–16677.
5 D. Maiti, X. Tong, X. Mou and K. Yang, *Front. Pharmacol.*, 2019, **9**, 1401.
6 Y. Xie, J. Rufo, R. Zhong, J. Rich, P. Li, K. W. Leong and T. J. Huang, *ACS Nano*, 2020, **14**, 16220–16240.
7 S. Z. Shirejini and F. Inci, *Biotechnol. Adv.*, 2022, **54**, 107814.
8 X. Ma, Y. Hao and L. Liu, *Int. J. Nanomed.*, 2021, **16**, 7575–7608.
9 W. Jiang, B. Y. S. Kim, J. T. Rutka and W. C. W. Chan, *Nat. Nanotechnol.*, 2008, **3**, 145–150.
10 A. Albanese, P. S. Tang and W. C. W. Chan, *Annu. Rev. Biomed. Eng.*, 2012, **14**, 1–16.
11 M. Wu, Z. Mao, K. Chen, H. Bachman, Y. Chen, J. Rufo, L. Ren, P. Li, L. Wang and T. J. Huang, *Adv. Funct. Mater.*, 2017, **27**, 1606039.
12 P. Arosio, T. Müller, L. Mahadevan and T. P. J. Knowles, *Nano Lett.*, 2014, **14**, 2365–2371.
13 M. A. Livshits, E. Khomyakova, E. G. Evtushenko, V. N. Lazarev, N. A. Kulemin, S. E. Semina, E. V. Generozov and V. M. Govorun, *Sci. Rep.*, 2015, **5**, 17319.
14 J. Lohwacharin and S. Takizawa, *J. Membr. Sci.*, 2009, **326**, 354–362.
15 G.-T. Wei and F.-K. Liu, *J. Chromatogr. A*, 1999, **836**, 253–260.
16 K. Y. Chung, J. M. Quek, S. H. Neo and H. P. Too, *J. Mol. Diagn.*, 2020, **22**, 610–618.
17 D. Brambilla, L. Sola, A. M. Ferretti, E. Chiodi, N. Zarovni, D. Fortunato, M. Criscuoli, V. Dolo, I. Giusti, V. Murdica, K. Kluszczyńska, L. Czernek, M. Düchler, R. Vago and M. Chiari, *Anal. Chem.*, 2021, **93**, 5476–5483.
18 A. Liga, A. D. B. Vliegenthart, W. Oosthuyzen, J. W. Dear and M. Kersaudy-Kerhoas, *Lab Chip*, 2015, **15**, 2388–2394.
19 G. M. Whitesides, *Nature*, 2006, **442**, 368–373.
20 J. C. Contreras-Naranjo, H.-J. Wu and V. M. Ugaz, *Lab Chip*, 2017, **17**, 3558–3577.
21 M. Sivaramakrishnan, R. Kothandan, D. K. Govindarajan, Y. Meganathan and K. Kandaswamy, *Curr. Opin. Biomed. Eng.*, 2020, **13**, 60–68.
22 S. Zhao, M. Wu, S. Yang, Y. Wu, Y. Gu, C. Chen, J. Ye, Z. Xie, Z. Tian, H. Bachman, P.-H. Huang, J. Xia, P. Zhang, H. Zhang and T. J. Huang, *Lab Chip*, 2020, **20**, 1298–1308.
23 M. Dimaki, M. H. Olsen, N. Rozlosnik and W. E. Svendsen, *Micromachines*, 2022, **13**, 866.
24 S. Khizar, H. Ben Halima, N. M. Ahmad, N. Zine, A. Errachid and A. Elaissari, *Electrophoresis*, 2020, **41**, 1206–1224.
25 H. Zhao, L. K. Chin, Y. Shi, P. Y. Liu, Y. Zhang, H. Cai, E. P. H. Yap, W. Ser and A.-Q. Liu, *Sens. Actuators, B*, 2021, **331**, 129428.
26 Q. Zhao, D. Yuan, J. Zhang and W. Li, *Micromachines*, 2020, **11**, 461.
27 M. Al-Fandi, M. Al-Rousan, M. A. K. Jaradat and L. Al-Ebbini, *Robot. Comput.-Integr. Manuf.*, 2011, **27**, 237–244.
28 Y. Cheng, Y. Wang, Z. Ma, W. Wang and X. Ye, *Lab Chip*, 2016, **16**, 4517–4526.
29 A. L. Vig and A. Kristensen, *Appl. Phys. Lett.*, 2008, **93**, 203507.
30 G. Romeo, G. D'Avino, F. Greco, P. A. Netti and P. L. Maffettone, *Lab Chip*, 2013, **13**, 2802–2807.
31 J. Zhou, P. Mukherjee, H. Gao, Q. Luan and I. Papautsky, *APL Bioeng.*, 2019, **3**, 041504.
32 S. Yan, J. Zhang, C. Pan, D. Yuan, G. Alici, H. Du, Y. Zhu and W. Li, *J. Micromech. Microeng.*, 2015, **25**, 084010.
33 H. Cha, H. Fallahi, Y. Dai, D. Yuan, H. An, N.-T. Nguyen and J. Zhang, *Lab Chip*, 2022, **22**, 423–444.

34 S. Lin, Z. Yu, D. Chen, Z. Wang, J. Miao, Q. Li, D. Zhang, J. Song and D. Cui, *Small*, 2020, **16**, 1903916.
35 S. Ibsen, A. Sonnenberg, C. Schutt, R. Mukthavaram, Y. Yeh, I. Ortac, S. Manouchehri, S. Kesari, S. Esener and M. J. Heller, *Small*, 2015, **11**, 5088–5096.
36 T. Salafi, K. K. Zeming and Y. Zhang, *Lab Chip*, 2016, **17**, 11–33.
37 M. Tayebi, Y. Zhou, P. Tripathi, R. Chandramohanadas and Y. Ai, *Anal. Chem.*, 2020, **92**, 10733–10742.
38 D. Yang, W. Zhang, H. Zhang, F. Zhang, L. Chen, L. Ma, L. M. Larcher, S. Chen, N. Liu, Q. Zhao, P. H. L. Tran, C. Chen, R. N. Veedu and T. Wang, *Theranostics*, 2020, **10**, 3684–3707.
39 J. Chen, P. Li, T. Zhang, Z. Xu, X. Huang, R. Wang and L. Du, *Front. Bioeng. Biotechnol.*, 2022, **9**, 811971.
40 F. Gao, F. Jiao, C. Xia, Y. Zhao, W. Ying, Y. Xie, X. Guan, M. Tao, Y. Zhang, W. Qin and X. Qian, *Chem. Sci.*, 2019, **10**, 1579–1588.
41 S. Cai, B. Luo, P. Jiang, X. Zhou, F. Lan, Q. Yi and Y. Wu, *Nanoscale*, 2018, **10**, 14280–14289.
42 L. Ding, X. Yang, Z. Gao, C. Y. Effah, X. Zhang, Y. Wu and L. Qu, *Small*, 2021, **17**, 2007174.
43 J. D. Robertson, L. Rizzello, M. Avila-Olias, J. Gaitzsch, C. Contini, M. S. Magoń, S. A. Renshaw and G. Battaglia, *Sci. Rep.*, 2016, **6**, 27494.
44 X. Sun, S. M. Tabakman, W.-S. Seo, L. Zhang, G. Zhang, S. Sherlock, L. Bai and H. Dai, *Angew. Chem., Int. Ed.*, 2009, **48**, 939–942.
45 W. Wang, J. Luo and S. Wang, *Adv. Healthcare Mater.*, 2018, **7**, 1800484.
46 H. Shao, H. Im, C. M. Castro, X. Breakefield, R. Weissleder and H. Lee, *Chem. Rev.*, 2018, **118**, 1917–1950.
47 C. Gardiner, D. D. Vizio, S. Sahoo, C. Théry, K. W. Witwer, M. Wauben and A. F. Hill, *J. Extracell. Vesicles*, 2016, **5**, 32945.
48 G. K. Patel, M. A. Khan, H. Zubair, S. K. Srivastava, M. Khushman, S. Singh and A. P. Singh, *Sci. Rep.*, 2019, **9**, 5335.
49 J. Wang, P. Ma, D. H. Kim, B.-F. Liu and U. Demirci, *Nano Today*, 2021, **37**, 101066.
50 C. Chen, J. Skog, C.-H. Hsu, R. T. Lessard, L. Balaj, T. Wurdinger, B. S. Carter, X. O. Breakefield, M. Toner and D. Irimia, *Lab Chip*, 2010, **10**, 505–511.
51 S.-C. Guo, S.-C. Tao and H. Dawn, *J. Extracell. Vesicles*, 2018, **7**, 1508271.
52 S. Benfer, P. Árki and G. Tomandl, *Adv. Eng. Mater.*, 2004, **6**, 495–500.
53 F. A. W. Coumans, A. R. Brisson, E. I. Buzas, F. Dignat-George, E. E. E. Drees, S. El-Andaloussi, C. Emanueli, A. Gasecka, A. Hendrix, A. F. Hill, R. Lacroix, Y. Lee, T. G. van Leeuwen, N. Mackman, I. Mäger, J. P. Nolan, E. van der Pol, D. M. Pegtel, S. Sahoo, P. R. M. Siljander, G. Sturk, O. de Wever and R. Nieuwland, *Circ. Res.*, 2017, **120**, 1632–1648.
54 X. Xiang, F. Guan, F. Jiao, H. Li, W. Zhang, Y. Zhang and W. Qin, *Anal. Methods*, 2021, **13**, 1591–1600.
55 R. J. Lobb, M. Becker, S. Wen Wen, C. S. F. Wong, A. P. Wiegmans, A. Leimgruber and A. Möller, *J. Extracell. Vesicles*, 2015, **4**, 27031.
56 L. Pitkänen and A. M. Striegel, *TrAC, Trends Anal. Chem.*, 2016, **80**, 311–320.
57 S. Süß, C. Metzger, C. Damm, D. Segets and W. Peukert, *Powder Technol.*, 2018, **339**, 264–272.
58 R. Stranska, L. Gysbrechts, J. Wouters, P. Vermeersch, K. Bloch, D. Dierickx, G. Andrei and R. Snoeck, *J. Transl. Med.*, 2018, **16**, 1.
59 C.-S. Hong, S. Funk, L. Muller, M. Boyiadzis and T. L. Whiteside, *J. Extracell. Vesicles*, 2016, **5**, 29289.
60 S. L. Shu, Y. Yang, C. L. Allen, E. Hurley, K. H. Tung, H. Minderman, Y. Wu and M. S. Ernstoff, *J. Extracell. Vesicles*, 2019, **9**, 1692401.
61 G. Sharma, A. Kumar, S. Sharma, Mu. Naushad, R. Prakash Dwivedi, Z. A. ALOthman and G. T. Mola, *J. King Saud Univ., Sci.*, 2019, **31**, 257–269.
62 G. Sharma, V. K. Gupta, S. Agarwal, A. Kumar, S. Thakur and D. Pathania, *J. Mol. Liq.*, 2016, **219**, 1137–1143.
63 P. Y. Reyes, J. A. Espinoza, M. E. Treviño, H. Saade and R. G. López, *J. Nanomater.*, 2010, **2010**, e948941.
64 Y. Dahman, in *Nanotechnology and Functional Materials for Engineers*, ed. Y. Dahman, Elsevier, 2017, pp. 121–144.
65 K. P. De Sousa, I. Rossi, M. Abdullahi, M. I. Ramirez, D. Stratton and J. M. Inal, *Wiley Interdiscip. Rev.: Nanomed. Nanobiotechnol.*, 2022, e1835.
66 L. Paolini, A. Zendrini, G. D. Noto, S. Busatto, E. Lottini, A. Radeghieri, A. Dossi, A. Caneschi, D. Ricotta and P. Bergese, *Sci. Rep.*, 2016, **6**, 23550.
67 Y. K. Yoo, J. Lee, H. Kim, K. S. Hwang, D. S. Yoon and J. H. Lee, *Micromachines*, 2018, **9**, 634.
68 C. F. Ruivo, B. Adem, M. Silva and S. A. Melo, *Cancer Res.*, 2017, **77**, 6480–6488.
69 M. L. Yarmush, A. M. Weiss, K. P. Antonsen, D. J. Odde and D. M. Yarmush, *Biotechnol. Adv.*, 1992, **10**, 413–446.
70 D. D. Taylor and S. Shah, *Methods*, 2015, **87**, 3–10.
71 C.-L. Shih, K.-Y. Chong, S.-C. Hsu, H.-J. Chien, C.-T. Ma, J. W.-C. Chang, C.-J. Yu and C.-C. Chiou, *New Biotechnol.*, 2016, **33**, 116–122.
72 J. Kowal, G. Arras, M. Colombo, M. Jouve, J. P. Morath, B. Primdal-Bengtson, F. Dingli, D. Loew, M. Tkach and C. Théry, *Proc. Natl. Acad. Sci. U. S. A.*, 2016, **113**, E968–E977.
73 Z. Andreu and M. Yáñez-Mó, *Front. Immunol.*, 2014, **5**, 442.
74 B. J. Tauro, D. W. Greening, R. A. Mathias, H. Ji, S. Mathivanan, A. M. Scott and R. J. Simpson, *Methods*, 2012, **56**, 293–304.
75 P. Sajeesh and A. K. Sen, *Microfluid. Nanofluid.*, 2014, **17**, 1–52.
76 L. Shi, A. Rana and L. Esfandiari, *Sci. Rep.*, 2018, **8**, 6751.
77 K. Mogi, K. Hayashida and T. Yamamoto, *Anal. Sci.*, 2018, **34**, 875–880.
78 P. Ohlsson, K. Petersson, P. Augustsson and T. Laurell, *Sci. Rep.*, 2018, **8**, 9156.
79 T. Yoon, H. S. Moon, J. W. Song, K. A. Hyun and H. I. Jung, *Cytometry, Part A*, 2019, **95**, 1135–1144.

80 E. Iswardy, T.-C. Tsai, I.-F. Cheng, T.-C. Ho, G. C. Perng and H.-C. Chang, *Biosens. Bioelectron.*, 2017, **95**, 174–180.
81 Y. Chen, M. Wu, L. Ren, J. Liu, P. H. Whitley, L. Wang and T. J. Huang, *Lab Chip*, 2016, **16**, 3466–3472.
82 D. J. Collins, Z. Ma, J. Han and Y. Ai, *Lab Chip*, 2016, **17**, 91–103.
83 K. Zhao and D. Li, *Sens. Actuators, B*, 2017, **250**, 274–284.
84 A. Lenshof and T. Laurell, in *Encyclopedia of Nanotechnology*, ed. B. Bhushan, Springer Netherlands, Dordrecht, 2014, pp. 1–6.
85 S. Mohanty, I. S. M. Khalil and S. Misra, *Proc. R. Soc. A*, 2020, **476**, 20200621.
86 Y. Xie, H. Bachman and T. J. Huang, *TrAC, Trends Anal. Chem.*, 2019, **117**, 280–290.
87 A. Fornell, K. Cushing, J. Nilsson and M. Tenje, *Appl. Phys. Lett.*, 2018, **112**, 063701.
88 L. Meng, F. Cai, F. Li, W. Zhou, L. Niu and H. Zheng, *J. Phys. D: Appl. Phys.*, 2019, **52**, 273001.
89 K. Länge, B. E. Rapp and M. Rapp, *Anal. Bioanal. Chem.*, 2008, **391**, 1509–1519.
90 I. Leibacher, P. Reichert and J. Dual, *Lab Chip*, 2015, **15**, 2896–2905.
91 Z. Chen, X. Liu, M. Kojima, Q. Huang and T. Arai, *Appl. Sci.*, 2020, **10**, 1260.
92 D. J. Collins, Z. Ma and Y. Ai, *Anal. Chem.*, 2016, **88**, 5513–5522.
93 L. Johansson, J. Enlund, S. Johansson, I. Katardjiev and V. Yantchev, *Biomed. Microdevices*, 2012, **14**, 279–289.
94 G. Destgeer, J. H. Jung, J. Park, H. Ahmed, K. Park, R. Ahmad and H. J. Sung, *RSC Adv.*, 2017, **7**, 22524–22530.
95 J. Shi, H. Huang, Z. Stratton, Y. Huang and T. J. Huang, *Lab Chip*, 2009, **9**, 3354–3359.
96 W. Connacher, N. Zhang, A. Huang, J. Mei, S. Zhang, T. Gopesh and J. Friend, *Lab Chip*, 2018, **18**, 1952–1996.
97 R. Weser, A. Winkler, M. Weihnacht, S. Menzel and H. Schmidt, *Ultrasonics*, 2020, **106**, 106160.
98 G. Destgeer, B. H. Ha, J. Park, J. H. Jung, A. Alazzam and H. J. Sung, *Phys. Procedia*, 2015, **70**, 34–37.
99 Y. Yang, L. Zhang, K. Jin, M. He, W. Wei, X. Chen, Q. Yang, Y. Wang, W. Pang, X. Ren and X. Duan, *Sci. Adv.*, 2022, **8**, eabn8440.
100 M. Wu, Y. Ouyang, Z. Wang, R. Zhang, P.-H. Huang, C. Chen, H. Li, P. Li, D. Quinn, M. Dao, S. Suresh, Y. Sadovsky and T. J. Huang, *Proc. Natl. Acad. Sci. U. S. A.*, 2017, **114**, 10584–10589.
101 F. Petersson, A. Nilsson, C. Holm, H. Jönsson and T. Laurell, *Lab Chip*, 2005, **5**, 20–22.
102 Y. Ai, C. K. Sanders and B. L. Marrone, *Anal. Chem.*, 2013, **85**, 9126–9134.
103 K. Lee, H. Shao, R. Weissleder and H. Lee, *ACS Nano*, 2015, **9**, 2321–2327.
104 M. Wu, A. Ozcelik, J. Rufo, Z. Wang, R. Fang and T. Jun Huang, *Microsyst. Nanoeng.*, 2019, **5**, 32.
105 M. Antfolk, P. B. Muller, P. Augustsson, H. Bruus and T. Laurell, *Lab Chip*, 2014, **14**, 2791–2799.
106 P. Ohlsson, M. Evander, K. Petersson, L. Mellhammar, A. Lehmusvuori, U. Karhunen, M. Soikkeli, T. Seppä, E. Tuunainen, A. Spangar, P. von Lode, K. Rantakokko-Jalava, G. Otto, S. Scheding, T. Soukka, S. Wittfooth and T. Laurell, *Anal. Chem.*, 2016, **88**, 9403–9411.
107 Y. Li, S. Cai, H. Shen, Y. Chen, Z. Ge and W. Yang, *Biomicrofluidics*, 2022, **16**, 031502.
108 Y. Gao, M. Wu, Y. Lin and J. Xu, *Micromachines*, 2020, **11**, E921.
109 K. D. Dorfman, in *Encyclopedia of Microfluidics and Nanofluidics*, ed. D. Li, Springer, New York, NY, 2015, pp. 926–934.
110 D. Li, in *Interface Science and Technology*, Elsevier, 2004, vol. 2, pp. 542–616.
111 X. Ou, P. Chen, X. Huang, S. Li and B.-F. Liu, *J. Sep. Sci.*, 2020, **43**, 258–270.
112 M. Dawod, N. E. Arvin and R. T. Kennedy, *Analyst*, 2017, **142**, 1847–1866.
113 K. D. Dorfman, S. B. King, D. W. Olson, J. D. P. Thomas and D. R. Tree, *Chem. Rev.*, 2013, **113**, 2584–2667.
114 E. O. Adekanmbi and S. K. Srivastava, *Lab Chip*, 2016, **16**, 2148–2167.
115 R. T. Davies, J. Kim, S. C. Jang, E.-J. Choi, Y. S. Gho and J. Park, *Lab Chip*, 2012, **12**, 5202–5210.
116 S. Marczak, K. Richards, Z. Ramshani, E. Smith, S. Senapati, R. Hill, D. B. Go and H.-C. Chang, *Electrophoresis*, 2018, **39**, 2029–2038.
117 B. Franze and C. Engelhard, *Anal. Chem.*, 2014, **86**, 5713–5720.
118 C. Adelantado, N. Rodríguez-Fariñas, R. C. Rodríguez Martín-Doimeadios, M. Zougagh and Á. Ríos, *Anal. Chim. Acta*, 2016, **923**, 82–88.
119 D.-T. Phan, S. A. M. Shaegh, C. Yang and N.-T. Nguyen, *Sens. Actuators, B*, 2016, **222**, 735–740.
120 S. Cho, W. Jo, Y. Heo, J. Y. Kang, R. Kwak and J. Park, *Sens. Actuators, B*, 2016, **233**, 289–297.
121 Y. Pan, S. Neuss, A. Leifert, M. Fischler, F. Wen, U. Simon, G. Schmid, W. Brandau and W. Jahnen-Dechent, *Small*, 2007, **3**, 1941–1949.
122 B. Kowalczyk, I. Lagzi and B. A. Grzybowski, *Curr. Opin. Colloid Interface Sci.*, 2011, **16**, 135–148.
123 M. Bouri, R. Salghi, M. Zougagh and A. Ríos, *Anal. Chem.*, 2013, **85**, 4858–4862.
124 S. Hassanpour Tamrin, A. Sanati Nezhad and A. Sen, *ACS Nano*, 2021, **15**, 17047–17079.
125 S. Grimnes and Ø. G. Martinsen, in *Bioimpedance and Bioelectricity Basics*, ed. S. Grimnes and Ø. G. Martinsen, Academic Press, Oxford, 3rd edn, 2015, pp. 179–254.
126 R. Pethig, *Biomicrofluidics*, 2010, **4**, 022811.
127 T. Ghomian and J. Hihath, *IEEE Trans. Biomed. Eng.*, 2022, 1–15.
128 C. Qian, H. Huang, L. Chen, X. Li, Z. Ge, T. Chen, Z. Yang and L. Sun, *Int. J. Mol. Sci.*, 2014, **15**, 18281–18309.
129 A. Alazzam, B. Mathew and F. Alhammadi, *J. Sep. Sci.*, 2017, **40**, 1193–1200.

130 R. Pethig, in *Dielectrophoresis*, John Wiley & Sons, Ltd, 2017, pp. 119–144.
131 E. A. Kwizera, M. Sun, A. M. White, J. Li and X. He, *ACS Biomater. Sci. Eng.*, 2021, **7**, 2043–2063.
132 H. Song, J. M. Rosano, Y. Wang, C. J. Garson, B. Prabhakarpandian, K. Pant, G. J. Klarmann, A. Perantoni, L. M. Alvarez and E. Lai, *Lab Chip*, 2015, **15**, 1320–1328.
133 H. Zhang, H. Chang and P. Neuzil, *Micromachines*, 2019, **10**, 423.
134 U. Kim, J. Qian, S. A. Kenrick, P. S. Daugherty and H. T. Soh, *Anal. Chem.*, 2008, **80**, 8656–8661.
135 L. Shi, D. Kuhnell, V. J. Borra, S. M. Langevin, T. Nakamura and L. Esfandiari, *Lab Chip*, 2019, **19**, 3726–3734.
136 S. Ayala-Mar, R. C. Gallo-Villanueva and J. González-Valdez, *Mater. Today: Proc.*, 2019, **13**, 332–340.
137 S. Ayala-Mar, V. H. Perez-Gonzalez, M. A. Mata-Gómez, R. C. Gallo-Villanueva and J. González-Valdez, *Anal. Chem.*, 2019, **91**, 14975–14982.
138 S. D. Ibsen, J. Wright, J. M. Lewis, S. Kim, S.-Y. Ko, J. Ong, S. Manouchehri, A. Vyas, J. Akers, C. C. Chen, B. S. Carter, S. C. Esener and M. J. Heller, *ACS Nano*, 2017, **11**, 6641–6651.
139 P. Modarres and M. Tabrizian, *Sens. Actuators, B*, 2017, **252**, 391–408.
140 L. Liu, K. Chen, N. Xiang and Z. Ni, *Electrophoresis*, 2019, **40**, 873–889.
141 S. Yaman, M. Anil-Inevi, E. Ozcivici and H. C. Tekin, *Front. Bioeng. Biotechnol.*, 2018, **6**, 192.
142 N.-T. Nguyen, *Microfluid. Nanofluid.*, 2012, **12**, 1–16.
143 M. D. Tarn, N. Hirota, A. Iles and N. Pamme, *Sci. Technol. Adv. Mater.*, 2009, **10**, 014611.
144 D. Robert, N. Pamme, H. Conjeaud, F. Gazeau, A. Iles and C. Wilhelm, *Lab Chip*, 2011, **11**, 1902–1910.
145 M. D. Krebs, R. M. Erb, B. B. Yellen, B. Samanta, A. Bajaj, V. M. Rotello and E. Alsberg, *Nano Lett.*, 2009, **9**, 1812–1817.
146 L. Zeng, X. Chen, J. Du, Z. Yu, R. Zhang, Y. Zhang and H. Yang, *Nanoscale*, 2021, **13**, 4029–4037.
147 L. Zeng, S. Hu, X. Chen, P. Zhang, G. Gu, Y. Wang, H. Zhang, Y. Zhang and H. Yang, *Lab Chip*, 2022, **22**, 2476–2488.
148 C. Park, J. Lee, Y. Kim, J. Kim, J. Lee and S. Park, *J. Microbiol. Methods*, 2017, **132**, 128–133.
149 Z. M. Wang, R. G. Wu, Z. P. Wang and R. V. Ramanujan, *Sci. Rep.*, 2016, **6**, 26945.
150 S. Oh, S. H. Jung, H. Seo, M.-K. Min, B. Kim, Y. K. Hahn, J. H. Kang and S. Choi, *Sens. Actuators, B*, 2018, **272**, 324–330.
151 Y. Liu, W. Zhao, R. Cheng, M. Logun, M. D. M. Zayas-Viera, L. Karumbaiah and L. Mao, *Lab Chip*, 2020, **20**, 3187–3201.
152 A. J. Mach, O. B. Adeyiga and D. D. Carlo, *Lab Chip*, 2013, **13**, 1011–1026.
153 S. S. Leong, Z. Ahmad, S. C. Low, J. Camacho, J. Faraudo and J. Lim, *Langmuir*, 2020, **36**, 8033–8055.
154 F. Alnaimat, S. Dagher, B. Mathew, A. Hilal-Alnqbi and S. Khashan, *Chem. Rec.*, 2018, **18**, 1596–1612.
155 P. Su, C. Ren, Y. Fu, J. Guo, J. Guo and Q. Yuan, *Sens. Actuators, A*, 2021, **332**, 113180.
156 A. Munaz, M. J. A. Shiddiky and N.-T. Nguyen, *Biomicrofluidics*, 2018, **12**, 031501.
157 P. Skupin-Mrugalska, P. A. Elvang and M. Brandl, *Int. J. Mol. Sci.*, 2021, **22**, 10456.
158 H. Kato, in *Characterization of Nanoparticles*, ed. V.-D. Hodoroaba, W. E. S. Unger and A. G. Shard, Elsevier, 2020, pp. 249–264.
159 A. Lenshof and T. Laurell, *Chem. Soc. Rev.*, 2010, **39**, 1203–1217.
160 J. C. Giddings, *Sep. Sci.*, 2006, 123–125.
161 C. Contado, *Anal. Bioanal. Chem.*, 2017, **409**, 2501–2518.
162 L. Calzolai, D. Gilliland, C. P. Garcìa and F. Rossi, *J. Chromatogr. A*, 2011, **1218**, 4234–4239.
163 H. Zhang, D. Freitas, H. S. Kim, K. Fabijanic, Z. Li, H. Chen, M. T. Mark, H. Molina, A. B. Martin, L. Bojmar, J. Fang, S. Rampersaud, A. Hoshino, I. Matei, C. M. Kenific, M. Nakajima, A. P. Mutvei, P. Sansone, W. Buehring, H. Wang, J. P. Jimenez, L. Cohen-Gould, N. Paknejad, M. Brendel, K. Manova-Todorova, A. Magalhães, J. A. Ferreira, H. Osório, A. M. Silva, A. Massey, J. R. Cubillos-Ruiz, G. Galletti, P. Giannakakou, A. M. Cuervo, J. Blenis, R. Schwartz, M. S. Brady, H. Peinado, J. Bromberg, H. Matsui, C. A. Reis and D. Lyden, *Nat. Cell Biol.*, 2018, **20**, 332–343.
164 J. Gigault, H. El Hadri, S. Reynaud, E. Deniau and B. Grassl, *Anal. Bioanal. Chem.*, 2017, **409**, 6761–6769.
165 B. Roda, A. Zattoni, P. Reschiglian, M. H. Moon, M. Mirasoli, E. Michelini and A. Roda, *Anal. Chim. Acta*, 2009, **635**, 132–143.
166 D. Kang, S. Oh, S.-M. Ahn, B.-H. Lee and M. H. Moon, *J. Proteome Res.*, 2008, **7**, 3475–3480.
167 J. S. Yang, J. C. Lee, S. K. Byeon, K. H. Rha and M. H. Moon, *Anal. Chem.*, 2017, **89**, 2488–2496.
168 J. C. Giddings, *Sep. Sci. Technol.*, 1985, **20**, 749–768.
169 A. De Momi and J. R. Lead, *Sci. Total Environ.*, 2008, **405**, 317–323.
170 A. De Momi and J. R. Lead, *Environ. Sci. Technol.*, 2006, **40**, 6738–6743.
171 A. Ashkin, *Phys. Rev. Lett.*, 1970, **24**, 156–159.
172 W. Wu, X. Zhu, Y. Zuo, L. Liang, S. Zhang, X. Zhang and Y. Yang, *ACS Photonics*, 2016, **3**, 2497–2504.
173 I. Fernandez-Cuesta, A. Llobera and M. Ramos-Payán, *Anal. Chim. Acta*, 2022, **1192**, 339307.
174 B. Landenberger, H. Höfemann, S. Wadle and A. Rohrbach, *Lab Chip*, 2012, **12**, 3177–3183.
175 P. Paiè, T. Zandrini, R. M. Vázquez, R. Osellame and F. Bragheri, *Micromachines*, 2018, **9**, 200.
176 F. Nan and Z. Yan, *Nano Lett.*, 2018, **18**, 7400–7406.
177 B. Ma, B. Yao, F. Peng, S. Yan, M. Lei and R. Rupp, *J. Opt.*, 2012, **14**, 105702.
178 H. Zhang and K.-K. Liu, *J. R. Soc., Interface*, 2008, **5**, 671–690.
179 B. R. Mutlu, J. F. Edd and M. Toner, *Proc. Natl. Acad. Sci. U. S. A.*, 2018, **115**, 7682–7687.
180 L. Wang and D. S. Dandy, *Adv. Sci.*, 2017, **4**, 1700153.

181 H. M. Tay, S. Y. Leong, X. Xu, F. Kong, M. Upadya, R. Dalan, C. Y. Tay, M. Dao, S. Suresh and H. W. Hou, *Lab Chip*, 2021, **21**, 2511–2523.
182 M. R. Condina, B. A. Dilmetz, S. R. Bazaz, J. Meneses, M. E. Warkiani and P. Hoffmann, *Lab Chip*, 2019, **19**, 1961–1970.
183 B. H. Wunsch, J. T. Smith, S. M. Gifford, C. Wang, M. Brink, R. L. Bruce, R. H. Austin, G. Stolovitzky and Y. Astier, *Nat. Nanotechnol.*, 2016, **11**, 936–940.
184 J. T. Smith, B. H. Wunsch, N. Dogra, M. E. Ahsen, K. Lee, K. K. Yadav, R. Weil, M. A. Pereira, J. V. Patel, E. A. Duch, J. M. Papalia, M. F. Lofaro, M. Gupta, A. K. Tewari, C. Cordon-Cardo, G. Stolovitzky and S. M. Gifford, *Lab Chip*, 2018, **18**, 3913–3925.
185 Y. Hattori, T. Shimada, T. Yasui, N. Kaji and Y. Baba, *Anal. Chem.*, 2019, **91**, 6514–6521.
186 Z. Han, C. Peng, J. Yi, D. Zhang, X. Xiang, X. Peng, B. Su, B. Liu, Y. Shen and L. Qiao, *Sens. Actuators, B*, 2021, **333**, 129563.
187 F. Inci, *Langmuir*, 2022, **38**, 1897–1909.
188 L.-G. Liang, M.-Q. Kong, S. Zhou, Y.-F. Sheng, P. Wang, T. Yu, F. Inci, W. P. Kuo, L.-J. Li, U. Demirci and S. Wang, *Sci. Rep.*, 2017, **7**, 46224.
189 S. Shin, D. Han, M. C. Park, J. Y. Mun, J. Choi, H. Chun, S. Kim and J. W. Hong, *Sci. Rep.*, 2017, **7**, 9907.
190 Y. Sai, M. Yamada, M. Yasuda and M. Seki, *J. Chromatogr. A*, 2006, **1127**, 214–220.
191 C. Liu, B. Ding, C. Xue, Y. Tian, G. Hu and J. Sun, *Anal. Chem.*, 2016, **88**, 12547–12553.
192 J. Y. Kim, S. W. Ahn, S. S. Lee and J. M. Kim, *Lab Chip*, 2012, **12**, 2807–2814.
193 C. Liu, J. Guo, F. Tian, N. Yang, F. Yan, Y. Ding, J. Wei, G. Hu, G. Nie and J. Sun, *ACS Nano*, 2017, **11**, 6968–6976.
194 J. Zhang, S. Yan, D. Yuan, G. Alici, N.-T. Nguyen, M. E. Warkiani and W. Li, *Lab Chip*, 2015, **16**, 10–34.
195 D. D. Carlo, *Lab Chip*, 2009, **9**, 3038–3046.
196 R. Nasiri, A. Shamloo, S. Ahadian, L. Amirifar, J. Akbari, M. J. Goudie, K. Lee, N. Ashammakhi, M. R. Dokmeci, D. Di Carlo and A. Khademhosseini, *Small*, 2020, **16**, 2000171.
197 W. Tang, S. Zhu, D. Jiang, L. Zhu, J. Yang and N. Xiang, *Lab Chip*, 2020, **20**, 3485–3502.
198 X. Lu, J. J. M. Chow, S. H. Koo, T. Y. Tan, B. Jiang and Y. Ai, *Anal. Chem.*, 2020, **92**, 15579–15586.
199 M. Li, M. van Zee, K. Goda and D. D. Carlo, *Lab Chip*, 2018, **18**, 2575–2582.
200 M. E. Warkiani, A. K. P. Tay, B. L. Khoo, X. Xiaofeng, J. Han and C. T. Lim, *Lab Chip*, 2015, **15**, 1101–1109.
201 D. Di Carlo, D. Irimia, R. G. Tompkins and M. Toner, *Proc. Natl. Acad. Sci. U. S. A.*, 2007, **104**, 18892–18897.
202 H. M. Tay, S. Kharel, R. Dalan, Z. J. Chen, K. K. Tan, B. O. Boehm, S. C. J. Loo and H. W. Hou, *NPG Asia Mater.*, 2017, **9**, e434–e434.
203 D. Huang, J. Man, D. Jiang, J. Zhao and N. Xiang, *Electrophoresis*, 2020, **41**, 2166–2187.
204 G.-Y. Kim, J.-I. Han and J.-K. Park, *BioChip J.*, 2018, **12**, 257–267.
205 Y. Gou, Y. Jia, P. Wang and C. Sun, *Sensors*, 2018, **18**, 1762.
206 H. Amini, W. Lee and D. D. Carlo, *Lab Chip*, 2014, **14**, 2739–2761.
207 Y. Deng, M. Kizer, M. Rada, J. Sage, X. Wang, D.-J. Cheon and A. J. Chung, *Nano Lett.*, 2018, **18**, 2705–2710.
208 A. J. Mach and D. Di Carlo, *Biotechnol. Bioeng.*, 2010, **107**, 302–311.
209 D. W. Inglis, J. A. Davis, R. H. Austin and J. C. Sturm, *Lab Chip*, 2006, **6**, 655–658.
210 A. Hochstetter, R. Vernekar, R. H. Austin, H. Becker, J. P. Beech, D. A. Fedosov, G. Gompper, S.-C. Kim, J. T. Smith, G. Stolovitzky, J. O. Tegenfeldt, B. H. Wunsch, K. K. Zeming, T. Krüger and D. W. Inglis, *ACS Nano*, 2020, **14**, 10784–10795.
211 J. A. Davis, *Doctor of Philosophy*, Princeton University, 2008.
212 S. Ranjan, K. K. Zeming, R. Jureen, D. Fisher and Y. Zhang, *Lab Chip*, 2014, **14**, 4250–4262.
213 L. R. Huang, E. C. Cox, R. H. Austin and J. C. Sturm, *Science*, 2004, **304**, 987–990.
214 E. Pariset, C. Parent, Y. Fouillet, B. François, N. Verplanck, F. Revol-Cavalier, A. Thuaire and V. Agache, *Sci. Rep.*, 2018, **8**, 17762.
215 K. K. Zeming, T. Salafi, C.-H. Chen and Y. Zhang, *Sci. Rep.*, 2016, **6**, 22934.
216 R. J. Gillams, V. Calero, R. Fernandez-Mateo and H. Morgan, *Lab Chip*, 2022, **22**, 3869–3876.
217 K. K. Zeming, N. V. Thakor, Y. Zhang and C.-H. Chen, *Lab Chip*, 2015, **16**, 75–85.
218 T. Salafi, Y. Zhang and Y. Zhang, *Nano-Micro Lett.*, 2019, **11**, 77.
219 J. McGrath, M. Jimenez and H. Bridle, *Lab Chip*, 2014, **14**, 4139–4158.
220 F. Liu, O. Vermesh, V. Mani, T. J. Ge, S. J. Madsen, A. Sabour, E.-C. Hsu, G. Gowrishankar, M. Kanada, J. V. Jokerst, R. G. Sierra, E. Chang, K. Lau, K. Sridhar, A. Bermudez, S. J. Pitteri, T. Stoyanova, R. Sinclair, V. S. Nair, S. S. Gambhir and U. Demirci, *ACS Nano*, 2017, **11**, 10712–10723.
221 H.-K. Woo, V. Sunkara, J. Park, T.-H. Kim, J.-R. Han, C.-J. Kim, H.-I. Choi, Y.-K. Kim and Y.-K. Cho, *ACS Nano*, 2017, **11**, 1360–1370.
222 S. Wang, D. Sarenac, M. H. Chen, S.-H. Huang, F. F. Giguel, D. R. Kuritzkes and U. Demirci, *Int. J. Nanomed.*, 2012, **7**, 5019–5028.
223 H. Bolze, J. Riewe, H. Bunjes, A. Dietzel and T. P. Burg, *Chem. Eng. Technol.*, 2021, **44**, 457–464.
224 I. Seder, H. Moon, S. J. Kang, S. Shin, W. J. Rhee and S.-J. Kim, *Lab Chip*, 2022, **22**, 3699–3707.
225 N. Debnath and M. Sadrzadeh, *J. Indian Inst. Sci.*, 2018, **98**, 137–157.
226 Y. Yoon, S. Kim, J. Lee, J. Choi, R.-K. Kim, S.-J. Lee, O. Sul and S.-B. Lee, *Sci. Rep.*, 2016, **6**, 26531.
227 S. Lin, Z. Yu, D. Chen, Z. Wang, J. Miao, Q. Li, D. Zhang, J. Song and D. Cui, *Small*, 2020, **16**, 1903916.
228 M. Yamada, M. Nakashima and M. Seki, *Anal. Chem.*, 2004, **76**, 5465–5471.

229 T. Morijiri, S. Sunahiro, M. Senaha, M. Yamada and M. Seki, *Microfluid. Nanofluid.*, 2011, **11**, 105–110.
230 H. W. Nho, N. Yang, J. Song, J. S. Park and T. H. Yoon, *Sens. Actuators, B*, 2017, **249**, 131–141.
231 S. Wang, Z. Liu, S. Wu, H. Sun, W. Zeng, J. Wei, Z. Fan, Z. Sui, L. Liu and X. Pan, *Electrophoresis*, 2021, **42**, 2223–2229.
232 A. Vig Larsen, L. Poulsen, H. Birgens, M. Dufva and A. Kristensen, *Lab Chip*, 2008, **8**, 818–821.
233 T. Hamacher, J. T. W. Berendsen, J. E. van Dongen, R. M. van der Hee, J. J. L. M. Cornelissen, M. L. W. J. Broekhuijse and L. I. Segerink, *Lab Chip*, 2021, **21**, 4477–4486.
234 N. Nivedita and I. Papautsky, *Biomicrofluidics*, 2013, **7**, 054101.
235 A. Jain and J. D. Posner, *Anal. Chem.*, 2008, **80**, 1641–1648.
236 D. Stoecklein and D. Di Carlo, *Anal. Chem.*, 2019, **91**, 296–314.
237 N. Xiang, X. Zhang, Q. Dai, J. Cheng, K. Chen and Z. Ni, *Lab Chip*, 2016, **16**, 2626–2635.
238 J. Zhou and I. Papautsky, *Microsyst. Nanoeng.*, 2020, **6**, 1–24.
239 Y. Zhou, Z. Ma and Y. Ai, *Lab Chip*, 2020, **20**, 568–581.
240 K. W. Seo, H. J. Byeon, H. K. Huh and S. J. Lee, *RSC Adv.*, 2013, **4**, 3512–3520.
241 A. M. Leshansky, A. Bransky, N. Korin and U. Dinnar, *Phys. Rev. Lett.*, 2007, **98**, 234501.
242 S. Yang, J. Y. Kim, S. J. Lee, S. S. Lee and J. M. Kim, *Lab Chip*, 2011, **11**, 266–273.
243 G. Li, G. H. McKinley and A. M. Ardekani, *J. Fluid Mech.*, 2015, **785**, 486–505.
244 J. Nam, H. Lim, D. Kim, H. Jung and S. Shin, *Lab Chip*, 2012, **12**, 1347–1354.
245 D. Yuan, J. Zhang, R. Sluyter, Q. Zhao, S. Yan, G. Alici and W. Li, *Lab Chip*, 2016, **16**, 3919–3928.
246 C. Liu, J. Zhao, F. Tian, J. Chang, W. Zhang and J. Sun, *J. Am. Chem. Soc.*, 2019, **141**, 3817–3821.
247 M. A. Faridi, H. Ramachandraiah, I. Banerjee, S. Ardabili, S. Zelenin and A. Russom, *J. Nanobiotechnol.*, 2017, **15**, 3.
248 J. Nam, J. Yoon, H. Jee, W. S. Jang and C. S. Lim, *Adv. Mater. Technol.*, 2020, **5**, 2000612.
249 Y. Zhou, Z. Ma, M. Tayebi and Y. Ai, *Anal. Chem.*, 2019, **91**, 4577–4584.
250 F. Shiri, H. Feng, K. E. Petersen, H. Sant, G. T. Bardi, L. A. Schroeder, M. L. Merchant, B. K. Gale and J. L. Hood, *Sci. Rep.*, 2022, **12**, 6146.
251 U. Kim and H. T. Soh, *Lab Chip*, 2009, **9**, 2313–2318.
252 D. J. Collins, T. Alan and A. Neild, *Lab Chip*, 2014, **14**, 1595–1603.
253 M. Tayebi, D. Yang, D. J. Collins and Y. Ai, *Nano Lett.*, 2021, **21**, 6835–6842.
254 S. M. Santana, M. A. Antonyak, R. A. Cerione and B. J. Kirby, *Biomed. Microdevices*, 2014, **16**, 869–877.
255 C. Théry, K. W. Witwer, E. Aikawa, M. J. Alcaraz, J. D. Anderson, R. Andriantsitohaina, A. Antoniou, T. Arab, F. Archer, G. K. Atkin-Smith, D. C. Ayre, J.-M. Bach, D. Bachurski, H. Baharvand, L. Balaj, S. Baldacchino, N. N. Bauer, A. A. Baxter, M. Bebawy, C. Beckham, A. Bedina Zavec, A. Benmoussa, A. C. Berardi, P. Bergese, E. Bielska, C. Blenkiron, S. Bobis-Wozowicz, E. Boilard, W. Boireau, A. Bongiovanni, F. E. Borràs, S. Bosch, C. M. Boulanger, X. Breakefield, A. M. Breglio, M. Á. Brennan, D. R. Brigstock, A. Brisson, M. L. Broekman, J. F. Bromberg, P. Bryl-Górecka, S. Buch, A. H. Buck, D. Burger, S. Busatto, D. Buschmann, B. Bussolati, E. I. Buzás, J. B. Byrd, G. Camussi, D. R. Carter, S. Caruso, L. W. Chamley, Y.-T. Chang, C. Chen, S. Chen, L. Cheng, A. R. Chin, A. Clayton, S. P. Clerici, A. Cocks, E. Cocucci, R. J. Coffey, A. Cordeiro-da-Silva, Y. Couch, F. A. Coumans, B. Coyle, R. Crescitelli, M. F. Criado, C. D'Souza-Schorey, S. Das, A. Datta Chaudhuri, P. de Candia, E. F. De Santana, O. De Wever, H. A. del Portillo, T. Demaret, S. Deville, A. Devitt, B. Dhondt, D. Di Vizio, L. C. Dieterich, V. Dolo, A. P. D. Rubio, M. Dominici, M. R. Dourado, T. A. Driedonks, F. V. Duarte, H. M. Duncan, R. M. Eichenberger, K. Ekström, S. E. L. Andaloussi, C. Elie-Caille, U. Erdbrügger, J. M. Falcón-Pérez, F. Fatima, J. E. Fish, M. Flores-Bellver, A. Försönits, A. Frelet-Barrand, F. Fricke, G. Fuhrmann, S. Gabrielsson, A. Gámez-Valero, C. Gardiner, K. Gärtner, R. Gaudin, Y. S. Gho, B. Giebel, C. Gilbert, M. Gimona, I. Giusti, D. C. Goberdhan, A. Görgens, S. M. Gorski, D. W. Greening, J. C. Gross, A. Gualerzi, G. N. Gupta, D. Gustafson, A. Handberg, R. A. Haraszti, P. Harrison, H. Hegyesi, A. Hendrix, A. F. Hill, F. H. Hochberg, K. F. Hoffmann, B. Holder, H. Holthofer, B. Hosseinkhani, G. Hu, Y. Huang, V. Huber, S. Hunt, A. G.-E. Ibrahim, T. Ikezu, J. M. Inal, M. Isin, A. Ivanova, H. K. Jackson, S. Jacobsen, S. M. Jay, M. Jayachandran, G. Jenster, L. Jiang, S. M. Johnson, J. C. Jones, A. Jong, T. Jovanovic-Talisman, S. Jung, R. Kalluri, S. Kano, S. Kaur, Y. Kawamura, E. T. Keller, D. Khamari, E. Khomyakova, A. Khvorova, P. Kierulf, K. P. Kim, T. Kislinger, M. Klingeborn, D. J. Klinke, M. Kornek, M. M. Kosanović, Á. F. Kovács, E.-M. Krämer-Albers, S. Krasemann, M. Krause, I. V. Kurochkin, G. D. Kusuma, S. Kuypers, S. Laitinen, S. M. Langevin, L. R. Languino, J. Lannigan, C. Lässer, L. C. Laurent, G. Lavieu, E. Lázaro-Ibáñez, S. Le Lay, M.-S. Lee, Y. X. F. Lee, D. S. Lemos, M. Lenassi, A. Leszczynska, I. T. Li, K. Liao, S. F. Libregts, E. Ligeti, R. Lim, S. K. Lim, A. Linē, K. Linnemannstöns, A. Llorente, C. A. Lombard, M. J. Lorenowicz, Á. M. Lörincz, J. Lötvall, J. Lovett, M. C. Lowry, X. Loyer, Q. Lu, B. Lukomska, T. R. Lunavat, S. L. Maas, H. Malhi, A. Marcilla, J. Mariani, J. Mariscal, E. S. Martens-Uzunova, L. Martin-Jaular, M. C. Martinez, V. R. Martins, M. Mathieu, S. Mathivanan, M. Maugeri, L. K. McGinnis, M. J. McVey, D. G. Meckes, K. L. Meehan, I. Mertens, V. R. Minciacchi, A. Möller, M. Møller Jørgensen, A. Morales-Kastresana, J. Morhayim, F. Mullier, M. Muraca, L. Musante, V. Mussack, D. C. Muth, K. H. Myburgh, T. Najrana, M. Nawaz, I. Nazarenko, P. Nejsum, C. Neri, T. Neri, R. Nieuwland, L. Nimrichter, J. P. Nolan, E. N. Nolte-'t Hoen, N. N. Hooten, L. O'Driscoll, T. O'Grady, A. O'Loghlen, T. Ochiya, M. Olivier, A. Ortiz, L. A. Ortiz, X. Osteikoetxea, O. Østergaard, M. Ostrowski, J. Park, D. M. Pegtel, H. Peinado, F. Perut, M. W. Pfaffl, D. G. Phinney, B. C. Pieters, R. C. Pink, D. S.

Pisetsky, E. P. von Strandmann, I. Polakovicova, I. K. Poon, B. H. Powell, I. Prada, L. Pulliam, P. Quesenberry, A. Radeghieri, R. L. Raffai, S. Raimondo, J. Rak, M. I. Ramirez, G. Raposo, M. S. Rayyan, N. Regev-Rudzki, F. L. Ricklefs, P. D. Robbins, D. D. Roberts, S. C. Rodrigues, E. Rohde, S. Rome, K. M. Rouschop, A. Rughetti, A. E. Russell, P. Saá, S. Sahoo, E. Salas-Huenuleo, C. Sánchez, J. A. Saugstad, M. J. Saul, R. M. Schiffelers, R. Schneider, T. H. Schøyen, A. Scott, E. Shahaj, S. Sharma, O. Shatnyeva, F. Shekari, G. V. Shelke, A. K. Shetty, K. Shiba, P. R.-M. Siljander, A. M. Silva, A. Skowronek, O. L. Snyder, R. P. Soares, B. W. Sódar, C. Soekmadji, J. Sotillo, P. D. Stahl, W. Stoorvogel, S. L. Stott, E. F. Strasser, S. Swift, H. Tahara, M. Tewari, K. Timms, S. Tiwari, R. Tixeira, M. Tkach, W. S. Toh, R. Tomasini, A. C. Torrecilhas, J. P. Tosar, V. Toxavidis, L. Urbanelli, P. Vader, B. W. van Balkom, S. G. van der Grein, J. Van Deun, M. J. van Herwijnen, K. Van Keuren-Jensen, G. van Niel, M. E. van Royen, A. J. van Wijnen, M. H. Vasconcelos, I. J. Vechetti, T. D. Veit, L. J. Vella, É. Velot, F. J. Verweij, B. Vestad, J. L. Viñas, T. Visnovitz, K. V. Vukman, J. Wahlgren, D. C. Watson, M. H. Wauben, A. Weaver, J. P. Webber, V. Weber, A. M. Wehman, D. J. Weiss, J. A. Welsh, S. Wendt, A. M. Wheelock, Z. Wiener, L. Witte, J. Wolfram, A. Xagorari, P. Xander, J. Xu, X. Yan, M. Yáñez-Mó, H. Yin, Y. Yuana, V. Zappulli, J. Zarubova, V. Žėkas, J. Zhang, Z. Zhao, L. Zheng, A. R. Zheutlin, A. M. Zickler, P. Zimmermann, A. M. Zivkovic, D. Zocco and E. K. Zuba-Surma, *J. Extracell. Vesicles*, 2018, **7**, 1535750.

256 M. Winey, J. B. Meehl, E. T. O'Toole and T. H. Giddings, *Mol. Biol. Cell*, 2014, **25**, 319–323.

257 K. Akhtar, S. A. Khan, S. B. Khan and A. M. Asiri, in *Handbook of Materials Characterization*, ed. S. K. Sharma, Springer International Publishing, Cham, 2018, pp. 113–145.

258 Y.-S. Chen, C. Chen, C. P.-K. Lai and G.-B. Lee, *Sens. Actuators, B*, 2022, **358**, 131473.

259 B. Lee, S. Yoon, J. W. Lee, Y. Kim, J. Chang, J. Yun, J. C. Ro, J.-S. Lee and J. H. Lee, *ACS Nano*, 2020, **14**, 17125–17133.

260 A. E. Vladár and V.-D. Hodoroaba, in *Characterization of Nanoparticles*, ed. V.-D. Hodoroaba, W. E. S. Unger and A. G. Shard, Elsevier, 2020, pp. 7–27.

261 E. Buhr, N. Senftleben, T. Klein, D. Bergmann, D. Gnieser, C. G. Frase and H. Bosse, *Meas. Sci. Technol.*, 2009, **20**, 084025.

262 P. M. Carvalho, M. R. Felício, N. C. Santos, S. Gonçalves and M. M. Domingues, *Front. Chem.*, 2018, **6**, 237.

263 J. Lim, S. P. Yeap, H. X. Che and S. C. Low, *Nanoscale Res. Lett.*, 2013, **8**, 381.

264 F. Caputo, J. Clogston, L. Calzolai, M. Rösslein and A. Prina-Mello, *J. Controlled Release*, 2019, **299**, 31–43.

265 A. P. Ramos, in *Nanocharacterization Techniques*, ed. A. L. Da Róz, M. Ferreira, F. de Lima Leite and O. N. Oliveira, William Andrew Publishing, 2017, pp. 99–110.

266 Y. H. Lai, S. Koo, S. H. Oh, E. A. Driskell and J. D. Driskell, *Anal. Methods*, 2015, **7**, 7249–7255.

267 S. Mourdikoudis, R. M. Pallares and N. T. K. Thanh, *Nanoscale*, 2018, **10**, 12871–12934.

268 P. Hole, K. Sillence, C. Hannell, C. M. Maguire, M. Roesslein, G. Suarez, S. Capracotta, Z. Magdolenova, L. Horev-Azaria, A. Dybowska, L. Cooke, A. Haase, S. Contal, S. Manø, A. Vennemann, J.-J. Sauvain, K. C. Staunton, S. Anguissola, A. Luch, M. Dusinska, R. Korenstein, A. C. Gutleb, M. Wiemann, A. Prina-Mello, M. Riediker and P. Wick, *J. Nanopart. Res.*, 2013, **15**, 2101.

269 V. Filipe, A. Hawe and W. Jiskoot, *Pharm. Res.*, 2010, **27**, 796–810.

270 E. van der Pol, F. A. W. Coumans, A. Sturk, R. Nieuwland and T. G. van Leeuwen, *Nano Lett.*, 2014, **14**, 6195–6201.

271 E. van der Pol, F. Coumans, Z. Varga, M. Krumrey and R. Nieuwland, *J. Thromb. Haemostasis*, 2013, **11**, 36–45.

272 R. A. Dragovic, C. Gardiner, A. S. Brooks, D. S. Tannetta, D. J. P. Ferguson, P. Hole, B. Carr, C. W. G. Redman, A. L. Harris, P. J. Dobson, P. Harrison and I. L. Sargent, *Nanomed.: Nanotechnol., Biol. Med.*, 2011, **7**, 780–788.

273 D. Bachurski, M. Schuldner, P.-H. Nguyen, A. Malz, K. S. Reiners, P. C. Grenzi, F. Babatz, A. C. Schauss, H. P. Hansen, M. Hallek and E. Pogge von Strandmann, *J. Extracell. Vesicles*, 2019, **8**, 1596016.

274 A. Rao, M. Schoenenberger, E. Gnecco, T. Glatzel, E. Meyer, D. Brändlin and L. Scandella, *J. Phys.: Conf. Ser.*, 2007, **61**, 971–976.

275 Y. Brill-Karniely, *Front. Bioeng. Biotechnol.*, 2020, **8**, 605153.

276 A. Calò, D. Reguera, G. Oncins, M.-A. Persuy, G. Sanz, S. Lobasso, A. Corcelli, E. Pajot-Augy and G. Gomila, *Nanoscale*, 2014, **6**, 2275–2285.

277 M. Krieg, G. Fläschner, D. Alsteens, B. M. Gaub, W. H. Roos, G. J. L. Wuite, H. E. Gaub, C. Gerber, Y. F. Dufrêne and D. J. Müller, *Nat. Rev. Phys.*, 2019, **1**, 41–57.

278 Y. F. Dufrêne, *Nat. Rev. Microbiol.*, 2008, **6**, 674–680.

279 X. Deng, F. Xiong, X. Li, B. Xiang, Z. Li, X. Wu, C. Guo, X. Li, Y. Li, G. Li, W. Xiong and Z. Zeng, *J. Nanobiotechnol.*, 2018, **16**, 102.

280 M. Li, N. Xi and L. Liu, *Nanoscale*, 2021, **13**, 8358–8375.

281 G. R. Heath, E. Kots, J. L. Robertson, S. Lansky, G. Khelashvili, H. Weinstein and S. Scheuring, *Nature*, 2021, **594**, 385–390.

282 C. M. Hoo, N. Starostin, P. West and M. L. Mecartney, *J. Nanopart. Res.*, 2008, **10**, 89–96.

283 Z. Zhao, Y. Yang, Y. Zeng and M. He, *Lab Chip*, 2016, **16**, 489–496.

284 S. S. Kanwar, C. J. Dunlay, D. M. Simeone and S. Nagrath, *Lab Chip*, 2014, **14**, 1891–1900.

285 S. Fang, H. Tian, X. Li, D. Jin, X. Li, J. Kong, C. Yang, X. Yang, Y. Lu, Y. Luo, B. Lin, W. Niu and T. Liu, *PLoS One*, 2017, **12**, e0175050.

286 X. Han, K. Xu, O. Taratula and K. Farsad, *Nanoscale*, 2019, **11**, 799–819.

287 A. Zuber, M. Purdey, E. Schartner, C. Forbes, B. van der Hoek, D. Giles, A. Abell, T. Monro and H. Ebendorff-Heidepriem, *Sens. Actuators, B*, 2016, **227**, 117–127.

288 M.-A. D'Hallewin, L. Bezdetnaya and F. Guillemin, *Eur. Urol.*, 2002, **42**, 417–425.
289 A.-L. Robson, P. C. Dastoor, J. Flynn, W. Palmer, A. Martin, D. W. Smith, A. Woldu and S. Hua, *Front. Pharmacol.*, 2018, **9**, 80.
290 Q.-L. Wang, W.-X. Huang, P.-J. Zhang, L. Chen, C.-K. Lio, H. Zhou, L.-S. Qing and P. Luo, *Microchim. Acta*, 2019, **187**, 61.
291 F. He, H. Liu, X. Guo, B.-C. Yin and B.-C. Ye, *Anal. Chem.*, 2017, **89**, 12968–12975.
292 H. Di, Z. Mi, Y. Sun, X. Liu, X. Liu, A. Li, Y. Jiang, H. Gao, P. Rong and D. Liu, *Theranostics*, 2020, **10**, 9303–9314.
293 Z. Chen, S.-B. Cheng, P. Cao, Q.-F. Qiu, Y. Chen, M. Xie, Y. Xu and W.-H. Huang, *Biosens. Bioelectron.*, 2018, **122**, 211–216.
294 R. Vaidyanathan, M. Naghibosadat, S. Rauf, D. Korbie, L. G. Carrascosa, M. J. A. Shiddiky and M. Trau, *Anal. Chem.*, 2014, **86**, 11125–11132.
295 E. Priyadarshini and N. Pradhan, *Sens. Actuators, B*, 2017, **238**, 888–902.
296 J. Xu and S. Wu, in *Nano-Inspired Biosensors for Protein Assay with Clinical Applications*, ed. G. Li, Elsevier, 2019, pp. 91–111.
297 M. G. Saad, H. Beyenal and W.-J. Dong, *Biosensors*, 2021, **11**, 518.
298 M. J. Kangas, R. M. Burks, J. Atwater, R. M. Lukowicz, P. Williams and A. E. Holmes, *Crit. Rev. Anal. Chem.*, 2017, **47**, 138–153.
299 Z. Li and M. Zhu, *Chem. Commun.*, 2020, **56**, 14541–14552.
300 S. Kwakye, V. N. Goral and A. J. Baeumner, *Biosens. Bioelectron.*, 2006, **21**, 2217–2223.
301 M. Safavieh, M. U. Ahmed, M. Tolba and M. Zourob, *Biosens. Bioelectron.*, 2012, **31**, 523–528.
302 T. Chen, C. Huang, Y. Wang and J. Wu, *Chin. Chem. Lett.*, 2022, **33**, 1180–1192.
303 Y.-G. Zhou, R. M. Mohamadi, M. Poudineh, L. Kermanshah, S. Ahmed, T. S. Safaei, J. Stojcic, R. K. Nam, E. H. Sargent and S. O. Kelley, *Small*, 2016, **12**, 727–732.
304 Q. Zhou, A. Rahimian, K. Son, D.-S. Shin, T. Patel and A. Revzin, *Methods*, 2016, **97**, 88–93.
305 B. J. Sanghavi, J. A. Moore, J. L. Chávez, J. A. Hagen, N. Kelley-Loughnane, C.-F. Chou and N. S. Swami, *Biosens. Bioelectron.*, 2016, **78**, 244–252.
306 Y. Wang, H. Xu, J. Luo, J. Liu, L. Wang, Y. Fan, S. Yan, Y. Yang and X. Cai, *Biosens. Bioelectron.*, 2016, **83**, 319–326.
307 S. R. Shin, T. Kilic, Y. S. Zhang, H. Avci, N. Hu, D. Kim, C. Branco, J. Aleman, S. Massa, A. Silvestri, J. Kang, A. Desalvo, M. A. Hussaini, S.-K. Chae, A. Polini, N. Bhise, M. A. Hussain, H. Lee, M. R. Dokmeci and A. Khademhosseini, *Adv. Sci.*, 2017, **4**, 1600522.
308 T. H. Fang, N. Ramalingam, D. Xian-Dui, T. S. Ngin, Z. Xianting, A. T. Lai Kuan, E. Y. Peng Huat and G. Hai-Qing, *Biosens. Bioelectron.*, 2009, **24**, 2131–2136.
309 D. Martín-Yerga, *Biosensors*, 2019, **9**, 47.
310 A. Sarkar, H. W. Hou, A. E. Mahan, J. Han and G. Alter, *Sci. Rep.*, 2016, **6**, 23589.
311 I. Bouhid de Aguiar and K. Schroën, *Membranes*, 2020, **10**, 316.
312 S. Y. Leong, H. B. Ong, H. M. Tay, F. Kong, M. Upadya, L. Gong, M. Dao, R. Dalan and H. W. Hou, *Small*, 2022, **18**, 2104470.
313 Y. Zhang, M. Chopp, Y. Meng, M. Katakowski, H. Xin, A. Mahmood and Y. Xiong, *J. Neurosurg.*, 2015, **122**, 856–867.
314 S. Dubascoux, F. Von Der Kammer, I. Le Hécho, M. P. Gautier and G. Lespes, *J. Chromatogr. A*, 2008, **1206**, 160–165.
315 C. Liu, H. Gong, W. Liu, B. Lu and L. Ye, *Ind. Eng. Chem. Res.*, 2019, **58**, 4695–4703.
316 S. C. Hur, H. T. K. Tse and D. D. Carlo, *Lab Chip*, 2010, **10**, 274–280.
317 H. Jeon, T. Kwon, J. Yoon and J. Han, *Lab Chip*, 2022, **22**, 272–285.
318 N. Xiang, R. Zhang, Y. Han and Z. Ni, *Anal. Chem.*, 2019, **91**, 5461–5468.
319 H. Ren, Z. Zhu, N. Xiang, H. Wang, T. Zheng, H. An, N.-T. Nguyen and J. Zhang, *Sens. Actuators, B*, 2021, **337**, 129758.